Monthly Notices of the ROYAL ASTRONOMICAL SOCIETY

MNRAS **530,** 2475–2495 (2024) https://doi.org/10.1093/mnras/stae854
Advance Access publication 2024 April 5

Looking for timing variations in the transits of 16 exoplanets

S. Yalçınkaya [1,2★] E. M. Esmer [1,2] Ö. Baştürk [1,2] A. Muhaymin [3] A. C. Kutluay [4] D. İ. Silistre,[3] F. Akar,[1] J. Southworth [5] L. Mancini [6,7,8] F. Davoudi,[9] E. Karamanlı,[3] F. Tezcan [10] E. Demir,[1] D. Yılmaz,[3] E. Güleroğlu [3] M. Tekin,[4] İ. Taşkın,[3] Y. Aladağ [11] E. Sertkan,[1] U. Y. Kurt [1] S. Fişek,[12] S. Kaptan [13] S. Aliş [12] N. Aksaker [11,14] F. K. Yelkenci [12] C. T. Tezcan [10,15] A. Kaya,[3] D. Oğlakkaya,[11] Z. S. Aydın[3] and C. Yeşilyaprak [10,15]

[1]*Department of Astronomy & Space Sciences, Faculty of Science, Ankara University, TR-06100 Ankara, Türkiye*
[2]*Astronomy and Space Sciences Research and Application Center (Kreiken Observatory), Ankara University, İncek Blvd., Ahlatlıbel, TR-06837 Ankara, Türkiye*
[3]*Department of Physics, Faculty of Science, Bilkent University, TR-06800 Ankara, Türkiye*
[4]*Physics Department, Science Faculty, Middle East Technical University,TR-06800 Ankara, Türkiye*
[5]*Astrophysics Group, Keele University, Staffordshire ST5 5BG, UK*
[6]*Department of Physics, University of Rome 'Tor Vergata', Via della Ricerca Scientifica 1, I-00133 Roma, Italy*
[7]*INAF – Turin Astrophysical Observatory, Via Osservatorio 20, I-10025 Pino Torinese, Italy*
[8]*Max Planck Institute for Astronomy, Königstuhl 17, D-69117 Heidelberg, Germany*
[9]*Astrobiology Research Unit, Universitè de Liège, Allèe du 6 Aôut 19C, B-4000 Liège, Belgium*
[10]*Department of Astronomy and Space Sciences, Science Faculty, Atatürk University, TR-25240 Erzurum, Türkiye*
[11]*Space Science and Solar Energy Research and Application Center (UZAYMER), University of Çukurova, TR-01330 Adana, Türkiye*
[12]*Department of Astronomy and Space Sciences, Faculty of Science, Istanbul University, TR-34119 Istanbul, Türkiye*
[13]*Astronomy and Space Sciences Program, Institute of Graduate Studies in Sciences, Istanbul University, TR-34116 Istanbul, Türkiye*
[14]*Adana Organised Industrial Zones Vocational School of Technical Science, University of Çukurova, TR-01410 Adana, Türkiye*
[15]*Atatürk University Astrophysics Research and Application Center (ATASAM), Yakutiye, TR-25240 Erzurum, Türkiye*

Accepted 2024 March 21. Received 2024 March 20; in original form 2023 August 10

ABSTRACT

We update the ephemerides of 16 transiting exoplanets using our ground-based observations, new *Transiting Exoplanet Survey Satellite* data, and previously published observations including those of amateur astronomers. All these light curves were modelled by making use of a set of quantitative criteria with the EXOFAST code to obtain mid-transit times. We searched for statistically significant secular and/or periodic trends in the mid-transit times. We found that the timing data are well modelled by a linear ephemeris for all systems except for XO-2 b, for which we detect an orbital decay with the rate of -12.95 ± 1.85 ms yr^{-1} that can be confirmed with future observations. We also detect a hint of potential periodic variations in the transit timing variation data of HAT-P-13 b, which also requires confirmation with further precise observations.

Key words: methods: observational – techniques: photometric – stars: individual: GJ 1214, HAT-P-1, HAT-P-10, HAT-P-13, HAT-P-16, HAT-P-22, HAT-P-30, HAT-P-53, KELT-3, QATAR-2, WASP-8, WASP-44, WASP-50, WASP-77A, WASP-93, and XO-2 – planetary systems.

1 INTRODUCTION

Since the observations of the first transits in an exoplanet system (Charbonneau et al. 2000), several questions have arisen regarding their formation, evolution, atmospheric composition, and orbital dynamics. These questions can be further investigated through different observational techniques. For example, radial velocity (RV) measurements during transits can be employed to determine the obliquity of a planet's orbit, which in turn can provide important information for improving theoretical models related to orbital evolution (Mancini et al. 2022). Occultation observations can provide information about the planet's energy budget (Arcangeli et al. 2021), while transmission spectroscopy can reveal its atmospheric composition (Maguire et al. 2023). However, these observations require high levels of precision, which can only be achieved by making use of large ground-based or space-borne telescopes. As the observation time for these instruments is in great demand, accurate predictions of transit and occultation times are crucial. Even small uncertainties in transit times can accumulate over time and require updates to the exoplanet's orbital period and reference mid-transit times (Mallonn et al. 2019).

Tidal interactions can cause the orbit of the planet to shrink (Maciejewski et al. 2016b). The period decrease per year may be much smaller than the uncertainty of the mid-transit times, making it difficult to observe. The amplitude of this effect increases over

★ E-mail: selcuk_yalcinkaya@yahoo.com

time and may be detected with additional transit (or occultation) observations over a long time range. In addition, transit timing analysis can be used to detect unseen additional bodies in a system that could not be seen with RV observations due to short phase coverage, stellar activity (Trifonov et al. 2021), or if the host star is too faint for precise RV observations (e.g. Gillon et al. 2017). For eccentric systems, the secular motion of the periastron (i.e. apsidal motion; Giménez & Bastero 1995) is observable with the help of occultation observations (Patra et al. 2017) and could give insights about tidal effects. To identify these effects using the transit timing variation (TTV) technique, it is essential to have transit timing measurements that cover longer time spans and are well sampled.

We selected potential periodic TTV targets depending on the known third bodies in the system or depending on their RV residuals.

In the potential TTV group, there are also orbital decay candidates selected based on their stellar and planetary radii, masses, and orbital separation and ages to work on systems with maximum tidal interaction potential. There are unitless metrics that are used to select our candidates (please see Baştürk et al. 2022). We observed 38 transits of 16 exoplanets (GJ 1214 b, HAT-P-1 b, HAT-P-10 b, HAT-P-13 b, HAT-P-16 b, HAT-P-22 b, HAT-P-30 b, HAT-P-53 b, KELT-3 b, QATAR-2 b, WASP-8 b, WASP-44 b, WASP-50 b, WASP-77A b, WASP-93 b, and XO-2 b) that we selected for their potential to display TTVs and/or large shifts in their observed transit timings.

The transit data that we used for timing calculation were obtained from ground-based telescopes and the *Transiting Exoplanet Survey Satellite* (*TESS*; Ricker et al. 2015), and compiled from published observations and open data bases.[1,2] We performed homogeneous transit timing analyses of these systems (listed in Table 1) and updated their ephemeris information.

This paper is organized as follows. In Section 2, we describe the telescopes and the detectors we used for transit observations, data reduction, and photometry procedure as well as light-curve selection criteria. TTV analyses and our results are presented in Section 3. We discuss our findings in Section 4.

2 OBSERVATIONS AND DATA REDUCTION

2.1 Observations

Photometric transit observations were carried out with the 1-m telescope located in TÜBİTAK National Observatory (T100), 80-cm telescope located in Ankara University Kreiken Observatory (T80), 50-cm telescope located in Atatürk University ATASAM Observatory (ATA50), 50-cm telescope located in Çukurova University UZAYMER Observatory (UT50), and 1.23m telescope of Calar Alto Observatory (CAHA). Detailed information about the telescopes and their detectors can be found in Baştürk et al. (2022). We also observed a multicolour transit of HAT-P-1 b with the Bonn University Simultaneous Camera on the CAHA 2.2-m telescope at the Observatory of Calar Alto (Spain). We made use of the well-established defocusing technique (Southworth et al. 2009) in order to increase photometric precision. Exposure times were set to acquire at least ∼50 frames per transit. The defocusing amount was determined to keep the detector response within its linearity limits while exposing it for larger durations to increase the signal-to-noise ratio (SNR) by reading out from a larger area. In general, we selected the photometric filter that gives the maximum SNR. A detailed log of photometric observations is provided in Table 2.

2.2 Data reduction

Data reduction (dark, bias, and flat correction) and ensemble aperture photometry were performed using the ASTROIMAGEJ (hereafter AIJ; Collins et al. 2017) software package. To increase the precision in photometry, we selected every star similar in brightness to the target in the field as a comparison; AIJ allows the user to visually inspect the relative flux of the target for a combination of different comparison stars. After finding suitable comparison stars, we experimented with different aperture sizes for both the stars and the sky background; AIJ also allows users to visually inspect relative flux change due to different aperture sizes. When selecting comparison stars and aperture sizes, our goal was to minimize the red noise, especially in contact times where the flux change is abrupt. Red noise during ingress and egress can change the mid-transit times dramatically, but may not affect the error bar of individual data points, which results in an underestimation of the mid-transit time uncertainty (Gillon et al. 2006; Pont, Zucker & Queloz 2006). This could lead to a higher reduced chi-square (χ^2_ν) for linear ephemeris, which could (incorrectly) be attributed to TTV. In order to avoid that, we detrended relative fluxes by using time-dependent variables such as airmass and target position on the CCD in an interactive manner using AIJ.

For *TESS* observations, we downloaded the 2-min light curves from Mikulski Archive for Space Telescopes[3] (MAST) that are processed by Science Processing Operations Center (SPOC) pipeline (Jenkins et al. 2016). SPOC generates presearch data conditioning (PDC) light curves and data validation time series (DVT) light curves using simple aperture photometry (SAP). The PDC_SAP fluxes are the corrected version of the SAP fluxes from instrumental systematics, outliers, and flux contamination from nearby stars. The DVT light curves are created by applying a running median filter to the PDC light curves to remove any long-term systematics and search for transits. We used only the DVT light curves because any signal other than transits will deteriorate the transit profiles, which in turn will increase the uncertainty in the measurement of the mid-transit times. For the case of XO-6 b, Ridden-Harper, Turner & Jayawardhana (2020) have shown that the DVT light curves have least scatter; nevertheless, the transit timings from DVT and PDC light curves are practically identical.

We have *TESS* light curves from the SPOC pipeline for all the planets in our sample except for HAT-P-53, which was observed by *TESS* during Sector 17, but light curves were not produced. Therefore, we downloaded the full frame images that have 30-min cadence from TESScut[4] and performed aperture photometry with the LIGHTKURVE package (Lightkurve Collaboration 2018) and then detrended the light curve using KEPLERSPLINE-V2[5] while ignoring the transit profiles. Final light curves were not suitable for individual modelling due to insufficient sampling, so we time-folded the data using a period from our preliminary analysis. We assumed the period of HAT-P-53 to be constant during Sector 17, but this enabled us to measure only a single mid-transit time from *TESS* observations. We included every *TESS* light curve until the end of the extended mission 2 (Sector 69) to our analysis.

[1] http://var2.astro.cz/ETD/index.php
[2] http://brucegary.net/AXA/x.htm
[3] https://mast.stsci.edu/portal/Mashup/Clients/Mast/Portal.html
[4] https://mast.stsci.edu/tesscut/
[5] https://github.com/avanderburg/keplersplinev2

Table 1. Fundamental stellar and planetary properties and the number of light curves analysed for each planetary system in our sample.

Planet name	$P_{\rm orb}$ (d)	$M_{\rm p}/M_{\star} \times 10^{-3}$	$T_{\rm eff,\star}$ (K)	Data base LC number	Literature LC number	Our LC number	*TESS* LC number	*Kepler* LC number	Total
GJ 1214 b[a]	1.580 3925(117)	0.157 ± 0.019	3026 ± 130	6	37	5	–	–	48
HAT-P-1 b[b]	4.465 29(9)	1.12 ± 0.09	5975 ± 45	2	7	5	12	–	26
HAT-P-10 b[c]	3.722 4747(65)	0.83 ± 0.03	4980 ± 60	16	7	2	4	–	29
HAT-P-13 b[d]	2.916 260(10)	1.22 ± 0.10	5653 ± 90	5	19	3	8	–	35
HAT-P-16 b[e]	2.775 96(3)	3.29 ± 0.13	6158 ± 80	35	11	2	14	–	62
HAT-P-22 b[f]	3.212 220(9)	0.916 ± 0.035	5302 ± 80	5	4	2	14	–	25
HAT-P-30 b[g]	2.810 595(5)	1.242 ± 0.041	6304 ± 88	19	5	–	24	–	48
HAT-P-53 b[h]	1.961 6241(39)	1.093 ± 0.043	5956 ± 50	7	3	2	1	–	13
KELT-3 b[i]	2.703 3904(100)	1.278 ± 0.063	6306 ± 50	7	1	1	17	–	26
QATAR-2 b[j]	1.337 1182(37)	0.740 ± 0.037	4645 ± 50	8	19	1	–	56	84
WASP-8 b[k]	8.158 715(16)	1.030 ± 0.061	5600 ± 80	1	2	–	6	–	7
WASP-44 b[l]	2.423 8039(87)	0.951 ± 0.034	5410 ± 150	13	11	1	8	–	33
WASP-50 b[m]	1.955 0959(51)	0.892 ± 0.080	5400 ± 100	19	13	2	20	–	54
WASP-77 b[n]	1.360 0309(20)	1.002 ± 0.045	5500 ± 80	13	6	2	32	–	53
WASP-93 b[o]	2.732 5321(20)	0.65 ± 0.06	6700 ± 100	5	4	7	6	–	22
XO-2 b[p]	2.615 857(5)	0.55 ± 0.07	5340 ± 32	13	9	3	18	–	42
Total				174	158	38	184	56	607

[a]Charbonneau et al. (2009).
[b]Bakos et al. (2007).
[c]Bakos et al. (2009a).
[d]Bakos et al. (2009b).
[e]Buchhave et al. (2010).
[f]Bakos et al. (2011).
[g]Johnson et al. (2011).
[h]Bonomo et al. (2017).
[i]Pepper et al. (2013).
[j]Bryan et al. (2012).
[k]Queloz et al. (2010).
[l]Anderson et al. (2012).
[m]Gillon et al. (2011).
[n]Maxted et al. (2013).
[o]Hay et al. (2016).
[p]Burke et al. (2007).

2.3 Light-curve selection criteria

The main goal of this work is to search for TTVs in the planetary systems listed in Table 1. This requires precise and accurate mid-transit times measured from high-quality light curves. For this reason, we used the light-curve selection criteria given in Başturk et al. (2022) to select suitable light curves. First, we compiled available transit light curves from literature, open data bases of amateur astronomers (Exoplanet Transit Database,[6] hereafter ETD, Poddaný et al. 2010, and Amateur Exoplanet Archive,[7] hereafter AXA) along with our own observations and observations from space telescopes (*TESS* and *Kepler Space Telescope*'s extended mission K2; Howell et al. 2014). We did not include light curves that have large gaps inside transit profiles or high-amplitude signatures of correlated noise, especially in the ingress or egress segments. Then, we modelled light curves with the EXOFAST (Eastman, Gaudi & Agol 2013) (see Section 3 for details) and then calculated photometric noise rate (PNR; Fulton et al. 2011b) from residuals, which indicates white noise. We removed the light curves that have PNR values higher than the transit depth. We binned the residuals between the ingress/egress duration ±5 min with 1-min steps and calculated the well-known β-values as defined in Winn et al. (2008) as a red noise indicator. We removed the light curves with the median β-value larger than 2.5. We also removed the light curves if the transit depth was a 5σ outlier for the given planet. When we visually inspect the removed light curves, we find that this criterion is very useful to detect problematic light curves. QATAR-2 b is an exception because it has K2 light curves with incomparably higher precision than other data sets, affecting the σ-value dramatically. Thus, we did not include depth values from K2 for QATAR-2 in the calculations of its 5σ level.

3 DATA ANALYSIS AND RESULTS

3.1 Light-curve modelling and measurements of mid-transit times

We followed the same method given in Başturk et al. (2022) to model the light curves and measure the mid-transit times. Briefly, we used EXOFAST-V1 to model the light curves after converting the observation time to Dynamical Barycentric Julian days (BJD-TDB) and detrending the light curves for the airmass effect that needed it with the AIJ. We used our scripts to convert the timings to BJD-TDB and calculated the airmass values by using relevant modules and functions of the ASTROPY (Astropy Collaboration 2013, 2018) library. The centres and widths of the priors were automatically selected from the NASA Exoplanet Archive[8] for the atmospheric

[6]http://var2.astro.cz/ETD/index.php
[7]http://brucegary.net/AXA/x.htm
[8]https://exoplanetarchive.ipac.caltech.edu/

Table 2. The log of photometric observations performed for this study. The dates of the light curves that are eliminated and hence not used in the TTV diagrams are marked and the reasons for their elimination are given in the footnotes.

System name	Telescope	Date UTC	Start UTC	End UTC	Filter	Exp. time (s)	Image number	PNR	β	Mid-transit BJD-TDB	Error (d)
GJ 1214	T100	2020-06-11	19:38:36	21:45:17	*R*	55	112	3.52	1.12	2459012.360728	0.000 376
GJ 1214	T100	2020-07-03	23:07:27	00:58:24	*I*	70	81	3.00	2.08	2459034.486291	0.000 454
GJ 1214	T100	2021-04-23	21:59:36	00:06:47	*I*	55	114	2.34	1.97	2459328.441673	0.000 261
GJ 1214	T100	2021-07-19[b]	19:06:03	22:04:02	*I*	60	142	2.60	2.00	2459415.362554	0.000 460
GJ 1214	T80	2022-05-12	22:42:10	00:55:10	i'	50	126	2.14	1.01	2455701.413994	0.000 224
HAT-P-1	ATA50	2022-09-15	17:42:12	01:46:02	z'	100	248	1.71	1.19	2456308.238083	0.000 464
HAT-P-1	CAHA (2.2 m)	2013-09-02	22:46:24	3:54:39	*u*	40	383	2.80	0.67	2456538.550339	0.000 526
HAT-P-1	CAHA (2.2 m)	2013-09-02	22:46:24	3:54:39	*b*	40	386	1.73	0.97	2456538.549978	0.000 314
HAT-P-1	CAHA (2.2 m)	2013-09-02	22:46:24	3:54:39	*y*	40	385	1.80	0.40	2456538.548745	0.000 327
HAT-P-1	CAHA (2.2 m)	2013-09-02	22:46:24	3:54:39	z'	40	381	1.30	0.76	2456538.549052	0.000 227
HAT-P-10	T100	2013-01-15	16:31:21	20:12:03	*R*	125	84	0.59	1.35	2456308.238083	0.000 203
HAT-P-10	T100	2020-10-25[c]	21:23:46	02:21:38	*R*	225	71	0.76	2.60	2459148.489796	0.000 421
HAT-P-13	CAHA (1.23 m)	2014-01-12	0:47:47	5:45:06	*R*	130	137	0.42	1.14	2456669.654639	0.000 429
HAT-P-13	CAHA (1.23 m)	2015-03-10	20:2:10	3:8:21	*R*	245	110	0.65	1.00	2457092.509213	0.000 445
HAT-P-13	T100	2021-01-03	18:34:21	01:37:17	*R*	245	100	0.38	1.49	2459218.452754	0.000 670
HAT-P-16	UT50	2020-10-21[a]	17:57:12	23:07:04	*R*	60	268	3.80	1.40	2459144.346886	0.000 759
HAT-P-16	ATA50	2020-10-07	21:21:53	02:17:13	*R*	185	93	0.76	2.02	2459130.474612	0.000 521
HAT-P-22	T100	2021-02-14	18:09:54	21:43:00	*R*	190	63	0.47	1.36	2459260.310347	0.000 313
HAT-P-22	T100	2014-02-17	22:50:43	03:29:44	*R*	185	80	0.85	1.57	2456706.584303	0.000 661
HAT-P-53	ATA50	2020-11-08[b]	15:28:21	19:38:48	*R*	170	73	5.20	1.33	2459162.237801	0.002 024
KELT-3	T100	2014-02-18	17:43:44	03:09:48	*R*	195	153	0.49	2.23	2456707.439231	0.000 560
QATAR-2	T100	2019-02-17	23:26:03	03:32:29	*R*	95	131	1.60	0.97	2458897.528172	0.000 234
WASP-44	T100	2020-08-27	21:47:53	01:22:40	*R*	125	87	1.52	1.05	2459089.484641	0.000 706
WASP-50	T100	2019-10-29	22:24:53	00:41:01	*R*	95	74	1.59	0.49	2458786.470867	0.000 405
WASP-50	T100	2020-10-09	23:03:08	01:53:44	*R*	105	79	0.96	0.65	2459132.522846	0.000 285
WASP-77	ATA50	2020-10-26	22:02:55	00:56:44	*R*	120	75	1.42	1.07	2459149.480906	0.000 526
WASP-77	ATA50	2021-10-16	21:08:02	01:05:21	*R*	115	106	1.13	1.21	2459504.447789	0.000 380
WASP-93	ATA50	2021-09-26	16:45:56	20:56:25	*R*	160	93	0.67	1.50	2459484.305639	0.000 726
WASP-93	UT50	2020-12-24	17:44:38	22:07:22	*R*	140	112	2.01	0.73	2459208.322251	0.001 692
WASP-93	T100	2020-01-12	17:01:44	20:55:19	*R*	145	88	0.78	1.61	2458861.287821	0.000 651
WASP-93	T100	2020-09-22[c]	20:35:59	01:50:32	*R*	200	89	0.58	2.70	2459115.413786	0.000 501
WASP-93	T100	2019-10-30	22:05:33	02:48:11	*R*	175	91	0.41	1.72	2458787.509779	0.000 421
WASP-93	T100	2020-11-24	16:35:48	20:37:04	*R*	105	119	1.18	1.32	2459178.263534	0.000 768
WASP-93	T100	2021-07-25[b]	21:06:17	01:28:45	*R*	140	101	0.96	1.61	2459421.461017	0.000 772
XO-2	T100	2020-01-12	22:18:58	03:16:03	*R*	175	94	1.36	1.89	2458861.528988	0.000 794
XO-2	T100	2020-12-25	20:07:25	01:06:58	*R*	220	78	0.61	2.47	2459209.437425	0.000 405
XO-2	UT50	2020-12-25	20:27:58	00:16:06	*R*	120	108	2.45	1.35	2459209.437700	0.000 9460

[a]Eliminated because it is an outlier on the TTV diagram.[b]Eliminated because its depth is out of 5σ of the average. [c]Eliminated because its β-factor is larger than 2.5.

parameters of the host stars as Gaussian priors and the orbital periods of the planets as constant values, while uniform priors of the limb darkening coefficients were automatically retrieved from Claret & Bloemen (2011) based on the atmospheric parameters of the host stars and the observed passbands. For the passbands that are not available, we choose the passband that has the closest transmission curve (e.g. we choose *I* for the *TESS* passband and Convection, Rotation and planetary Transits (CoRoT) for the clear observations).

After selecting the light curves as described in Section 2.3 and measuring the mid-transit times from the individual transit models using a built-in IDL routine AMOEBA that uses downhill simplex method (Nelder & Mead 1965) to minimize χ^2, we constructed the TTV diagrams and fitted a linear ephemeris using EMCEE (Foreman-Mackey et al. 2013) following the recipe given in Baştürk et al. (2022). We discarded the two-tailed 3σ outliers from the linear ephemeris not to bias our final results. These light curves with correlated noise, especially during ingress or egress, may survive the $\beta > 2.5$ criteria and result in an inaccurate mid-transit time with underestimated error bars. We visually inspected the light curves eliminated based on this criterion and we noticed that this criterion is especially useful for the light curves that come from spectroscopic observations (i.e. white light curve, formed by integrating an observed spectrum over the entire wavelength coverage) because these light curves usually have very high precision (hence low mid-transit time error) but inaccurate mid-transit times due to heavy detrending. We also noticed that this criterion enables us to detect light curves with incorrectly reported time references. We did not apply two-tailed 3σ outlier criteria for the XO-2 system because we detected a statistically significant orbital period decrease. For the QATAR-2 system, we calculated the 3σ value without including K2 light curves but a linear ephemeris was fitted to all data points including K2.

3.2 Ephemeris corrections

For all systems, we fitted independent linear and quadratic ephemeris using the EMCEE package. We followed the same procedure as described in Baştürk et al. (2022) for selecting random walkers, burn-in period, and Markov chain Monte Carlo steps for convergence. The median values of posterior probability distributions (PPDs) of linear elements slope and *y*-intercept were added to the reference period

Table 3. Reference ephemeris information (T_0 and P_{orb}).

Planet	T_0 (BJD_{TDB})	P_{orb} (d)
GJ 1214 b	2455799.398485(19)	1.580 404 418(58)
HAT-P-1 b	2454363.94778(13)	4.465 300 31(18)
HAT-P-10 b	2456933.615316(50)	3.722 479 75(13)
HAT-P-13 b	2456316.79044(12)	2.916 241 21(16)
HAT-P-16 b	2456204.604299(69)	2.775 967 270(90)
HAT-P-22 b	2454891.67399(13)	3.212 232 65(10)
HAT-P-30 b	2457775.212778(77)	2.810 600 70(13)
HAT-P-53 b	2458771.88605(28)	1.961 625 29(35)
KELT-3 b	2458872.854373(95)	2.703 390 23(43)
QATAR-2 b	2457218.1101306(63)	1.337 116 440(32)
WASP-8 b	2458375.23865(11)	8.158 725 62(67)
WASP-44 b	2458398.69812(13)	2.423 811 31(13)
WASP-50 b	2458411.093420(55)	1.955 092 447(48)
WASP-77A b	2458410.984807(28)	1.360 028 898(50)
WASP-93 b	2456079.56501(26)	2.732 537 78(25)
XO-2 b	2458843.218463(69)	2.615 859 462(54)

(P_{orb}) and mid-transit time (T_c), respectively. The updated linear ephemerides are listed in Table 3 with their uncertainties calculated from PPD.

3.3 Transit timing analyses

In order to detect potential secular changes in the orbital periods, we fitted quadratic functions to the TTVs of all planets using the method described in Section 3.2. We compared the quadratic ephemeris with the linear to detect any significant secular change for the planets in our sample.

In Table 4, we report the Akaike information criterion difference (ΔAIC) and Bayesian information criterion difference (ΔBIC) values between linear and quadratic ephemeris and the rate of the secular period change calculated from the coefficient of the second-degree term of the quadratic ephemeris. We only consider $\Delta BIC > 10$ as suggested strong evidence by Raftery (1995) to favour quadratic over the linear ephemerides.

After correcting the ephemerides (displayed in Fig. 1) using the linear coefficients, we performed a frequency analysis to search for potential periodic variations that can be caused by orbital perturbers or the apsidal motion of the planets. We used the ASTROPY's Lomb–Scargle function (VanderPlas 2018) to find possible frequencies and their false alarm probabilities (FAPs).

3.3.1 GJ 1214 system

GJ 1214 b is a sub-Neptune planet ($M_p = 6.55\ M_\oplus$ and $R_p = 2.678\ R_\oplus$) that orbits an M type dwarf star. It has a very high transmission spectroscopy metric (TSM; Kempton et al. 2018), making it one of the most favourable sub-Neptune planets for atmospheric studies (Charbonneau et al. 2009). Additional bodies in the system have been searched for using the RV method with 165 RV points spanning 10 yr (Cloutier et al. 2021), as well as with the transit method using a continuous observing run for ∼21 d from the *Spitzer Space Telescope* (Gillon et al. 2014). Follow-up transit observations have been performed multiple times to investigate TTVs or the atmospheric properties of the planet (Kundurthy et al. 2011; de Mooij et al. 2012; Harpsøe et al. 2013; Narita et al. 2013; Cáceres et al. 2014; Nascimbeni et al. 2015; Parviainen et al. 2015; Angerhausen et al. 2017; Rackham et al. 2017; Mallonn et al. 2018; Orell-Miquel et al. 2022; Spake et al. 2022; Gao et al. 2023; Lampón et al. 2023). We selected the planet for its potential to display TTVs as well as updating its ephemeris for future observation plans especially to understand its atmospheric properties.

We analysed a total of 48 light curves, including 6 from the ETD, 37 from the literature, and 5 from our observations. However, five of the light curves did not meet our selection criteria and were eliminated (as explained in Section 2.3). The total data span 10 yr of observations, but there was a 5-yr gap in the TTV diagram. After analysing the TTV diagram, we did not detect any significant period change in the GJ 1214 system.

3.3.2 HAT-P-1 system

HAT-P-1 b is a warm Jupiter with low density ($M_p = 0.53\ M_J$ and $R_p = 1.36\ R_J$) orbiting a G0 V-type star discovered by Bakos et al. (2007). The host star is part of a wide binary system with a companion (HAT-P-1A) of similar effective temperature, making it an excellent comparison star for atmospheric observations in high angular resolution. The planet has a relatively high TSM, which makes it a favourable object for atmospheric studies using ground-based and space-borne telescopes (e.g. Wakeford et al. 2013; Montalto et al. 2015). Bakos et al. (2007) suggested a small eccentricity that could be attributed to perturbations by an outer companion, which could be discovered by RV or TTV observations. With follow-up RV observations, Ment et al. (2018) rejected the eccentric orbit and Johnson et al. (2008) found that the spin of the orbit of HAT-P-1 b is aligned with the stellar rotation axis. Winn et al. (2007) and Johnson et al. (2008) found no significant TTVs in the system.

Here, we analysed 26 transit light curves, 3 of which were eliminated, to update the ephemeris of HAT-P-1 b. We found no statistically significant periodic or parabolic change in the period analysis. We updated the ephemeris of transit, which can be very useful for future atmospheric observations.

3.3.3 HAT-P-10/WASP-11 system

HAT-P-10 b is a low-mass, hot Jupiter that was independently discovered by Bakos et al. (2009a) and West et al. (2009). Follow-up RV observations by Knutson et al. (2014) revealed a linear trend that suggested the presence of a stellar-mass companion. Adaptive-optic (AO) observations by Ngo et al. (2015) revealed the existence of a 0.36-$M_\odot$ companion at a distance of 42 au (∼0.235 arcsec), which can explain the RV trend. Ngo et al. (2016) showed that the companion cannot cause Kozai–Lidov migration of the planet, and the eccentricity of the planet is consistent with zero as expected. The Rossiter–Mclaughlin (RM) observations by Mancini et al. (2015) indicate that the system is aligned, and this alignment has a primordial origin rather than being due to tidal interactions, owing to the relatively long distance between the star and the planet. Therefore, we do not expect to observe orbital decay in this system. Wang et al. (2014) investigated the TTVs to detect any outer companion with the light-time effect (LiTE), but found the orbital period of HAT-P-10 b to be constant. We included this system in our study for the same reasons and studied its TTV diagram with more data spanning a longer baseline.

We conducted an analysis of 29 transit light curves, consisting of 16 from ETD, 7 from literature, 4 from *TESS*, and 2 from our own observations. However, we excluded 4 of them and ultimately derived a TTV diagram from 25 mid-transit times that were evenly distributed across a span of 13 yr. Our analysis of the TTV diagram

Table 4. Lower limits for the reduced tidal quality factors ($Q'_\star$) for the host stars in our sample at 95 per cent confidence level. ΔAIC and ΔBIC values were used for comparisons between linear and quadratic models in this order. The quadratic model is favoured in the cases where ΔBIC > 10.

System	ΔAIC	ΔBIC	dP/dE (d/cycle)	$\dot{P}$ (ms yr^{-1})	$Q'_\star$
GJ 1214	− 1.58	− 3.32	6.63 ± 11.4 × 10^{-11}	1.32 ± 2.26	>2.4 × 10^2
HAT-P-1	− 1.90	− 3.00	− 3.63 ± 9.20 × 10^{-10}	18.99 ± 9.83	>6.2 × 10^2
HAT-P-10	0.63	− 0.54	− 9.60 ± 5.98 × 10^{-10}	− 8.14 ± 5.07	>4.1 × 10^2
HAT-P-13	− 2.52	− 3.86	− 1.98 ± 10.2 × 10^{-10}	− 2.14 ± 11.10	>1.1 × 10^5
HAT-P-16	− 1.62	− 3.59	− 3.35 ± 5.01 × 10^{-10}	− 8.93 ± 10.12	>2.6 × 10^4
HAT-P-22	1.07	2.02	1.14 ± 0.58 × 10^{-9}	11.24 ± 5.65	>2.4 × 10^3
HAT-P-30	1.66	− 0.08	− 1.32 ± 0.61 × 10^{-9}	− 43.8 ± 12.12	>1.6 × 10^3
HAT-P-53	− 0.42	− 0.61	2.0 ± 1.70 × 10^{-9}	32.30 ± 27.55	>8.2 × 10^3
KELT-3	− 0.13	− 0.90	2.12 ± 1.84 × 10^{-9}	24.72 ± 21.53	>8.8 × 10^3
QATAR-2	7.26	4.90	2.46 ± 0.80 × 10^{-10}	5.81 ± 1.89	>1.4 × 10^4
WASP-8	0.53	0.45	7.40 ± 4.76 × 10^{-9}	28.60 ± 18.40	>2.4 × 10^0
WASP-44	7.27	5.94	4.78 ± 1.13 × 10^{-9}	62.23 ± 14.69	>5.5 × 10^2
WASP-50	− 0.59	− 2.40	− 4.42 ± 3.60 × 10^{-10}	− 7.14 ± 5.81	>6.9 × 10^3
WASP-77A	0.15	− 1.63	− 1.69 ± 1.20 × 10^{-10}	− 3.93 ± 2.78	>7.2 × 10^4
WASP-93	− 1.07	− 2.28	− 7.87 ± 9.46 × 10^{-10}	− 31.89 ± 19.03	>3.7 × 10^3
XO-2	45.15	42.98	− 10.7 ± 1.54 × 10^{-10}	− 12.95 ± 1.85	=1.5 × 10^3

did not reveal any significant periodic changes or deviations from a constant period.

3.3.4 *HAT-P-13 system*

HAT-P-13 b is a warm Jupiter discovered by Bakos et al. (2009b), revolving around a solar-like, metal-rich {$T_{\rm eff}$ = 5653 K and [Fe/H] = 0.41}, and slightly evolved star. The system consists of at least another planet, HAT-P-13 c, highly eccentric (e = 0.691), long period ($P_{\rm c}$ = 446.27 d), massive ($M_{\rm p} \sin i$ = 15.2 $M_{\rm J}$) outer companion discovered with RV observations. The presence of another outer companion is suggested by the linear trend of RV residuals, as noted by Winn et al. (2010a) and Knutson et al. (2014). HAT-P-13 was suggested to have a cooler companion ($T_{\rm eff}$ = 3900 K; Piskorz et al. 2015) blending its lines in its infrared spectrum. However, the AO observations do not reveal a companion (Ngo et al. 2015), within the limits of the study given in their fig. 4 making the system worthwhile for TTV investigations. Nascimbeni et al. (2011) and Pál et al. (2011) suggested that the system has significant TTV, while Southworth et al. (2012), Fulton et al. (2011b), and Sada & Ramón-Fox (2016) found the period to be constant by ignoring a single outlier in the TTV diagram. Sun et al. (2023) detected apsidal motion of the orbit with a ΔBIC = 26.

We used 28 light curves to construct the TTV diagram of HAT-P-13 b, after eliminating 7 of them. We found that the period of HAT-P-13 b deviates from a constant period. The frequency analysis revealed a peak at 479.52 d with an FAP of 0.0007 and the full TTV amplitude is ∼321 s (see Fig. 2). Assuming that planet c is the perturber, and the system is coplanar, the TTV amplitude caused by a planet c should be approximately 40 s, as previously calculated by Bakos et al. (2009b). The RM observations by Winn et al. (2010a) revealed that the orbit of HAT-P-13 b is aligned, which supports the coplanar scenario. However, the transit of HAT-P-13 c has not been observed in long-term observations by Fulton et al. (2011b) and Szabó et al. (2010). Therefore, we conducted a preliminary Newtonian orbital analysis to fit the RVs and TTVs and found that the inclination of the putative planet c must be ∼2°, and its mass should be ∼0.4 $M_\odot$ to cause a 321-s TTV. If this is the case, we would expect the impact parameter, b, to vary over time, making HAT-P-13 b's orbit misaligned.

Some of the transit light curves of HAT-P-13 b exhibit modulations that can be attributed to star-spots. This makes it challenging to accurately measure the mid-transit times, which could introduce fallacious TTVs. Additional observations, including upcoming *TESS* data and new ground-based observations, are needed to determine the true ephemeris of HAT-P-13 b. We suggest that these light curves require special treatment, such as Gaussian process (Yalçınkaya et al. 2021) or spot modelling (Mancini et al. 2017), for better accuracy.

3.3.5 *HAT-P-16 system*

HAT-P-16 b is a dense ($M_{\rm p}$ = 4.193 $M_{\rm J}$ and $R_{\rm p}$ = 1.289 $R_{\rm J}$), hot Jupiter (P = 2.775 960 d) orbiting an F8 dwarf, discovered by Buchhave et al. (2010). The planet was found to have a small but statistically significant eccentricity based on its RV observations (Buchhave et al. 2010; Bonomo et al. 2017) and its projected spin–orbit angle suggests that it is aligned within the limits of measurement uncertainties (projected spin–orbit angle, $\lambda = -10° \pm 16°$; Moutou et al. 2011). The small eccentricity could be explained by the young age of the system (2 ± 0.8 Gyr: Buchhave et al. 2010; 0.5 ± 0.5 Gyr: Ciceri et al. 2013; 0.8 ± 0.2 Gyr: Bonfanti et al. 2015), which might be less than the tidal circularization time. However, the tidal circularization time is linearly dependent on the tidal quality factor ($Q_{\rm p}$; Adams & Laughlin 2006b) and it is not well known for hot Jupiters. The stellar age of the cold stars on the main sequence (MS) could not be precisely calculated with the isochrone fitting method because the change in their masses and radii during their MS evolution is comparable to the uncertainties on these parameters. Therefore, it is not possible to deduce the eccentricity of the orbit of HAT-P-16 b based on a comparison of the tidal circularization time with the stellar age. However, Knutson, Howard & Isaacson (2010) measured the $\log R'_{\rm HK}$ index as −4.863, which indicates low magnetic activity (e.g. Noyes et al. 1984), and Ciceri et al. (2013) found no star-spot-induced anomalies in the transit light curves, which is also indicative of low magnetic activity. Hence, the system should not be very young. Using the $\log(R'_{\rm HK})$−stellar rotation period ($P_{\rm rot}$) calibration from Suárez Mascareño et al. (2015), we found $P_{\rm rot}$ ∼ 22.5 d and $v_{\rm rot}$ = 2.8 km s^{-1}, meaning that the stellar inclination ($I_\star$) is consistent with 90° within uncertainties ($V \sin i$ = 3.5 ± 0.5; Buchhave et al. 2010). This result, combined with the RM values, suggests that the orbit of HAT-P-16 b is well

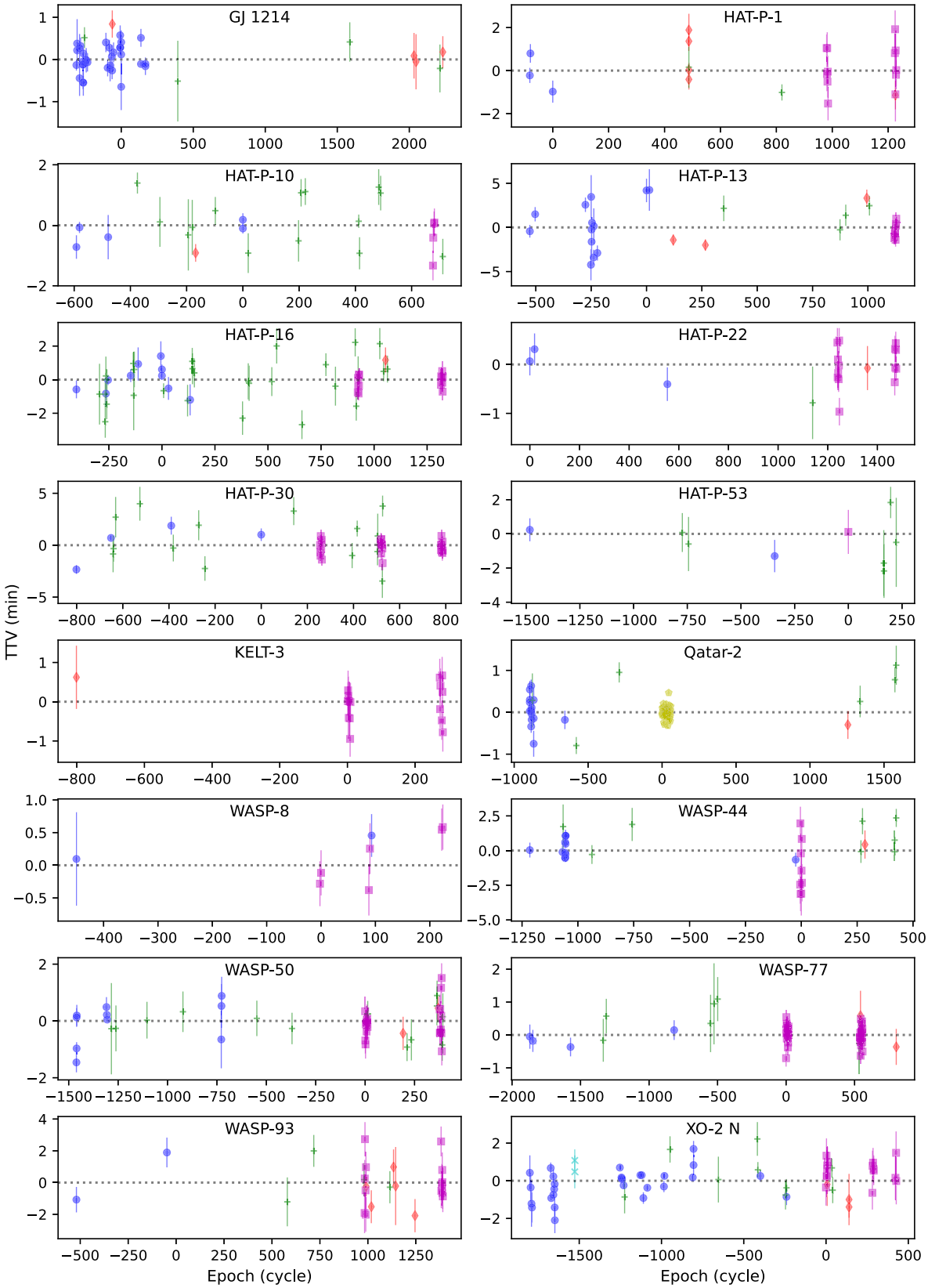

Figure 1. Linear residuals of TTV diagrams for all the planets in our sample based on observations from open data bases (plus symbol for ETD and x symbol for AXA), our observations (diamond), *TESS* observations (square), *Kepler* observations (pentagon), and light curves published in the literature (circle).

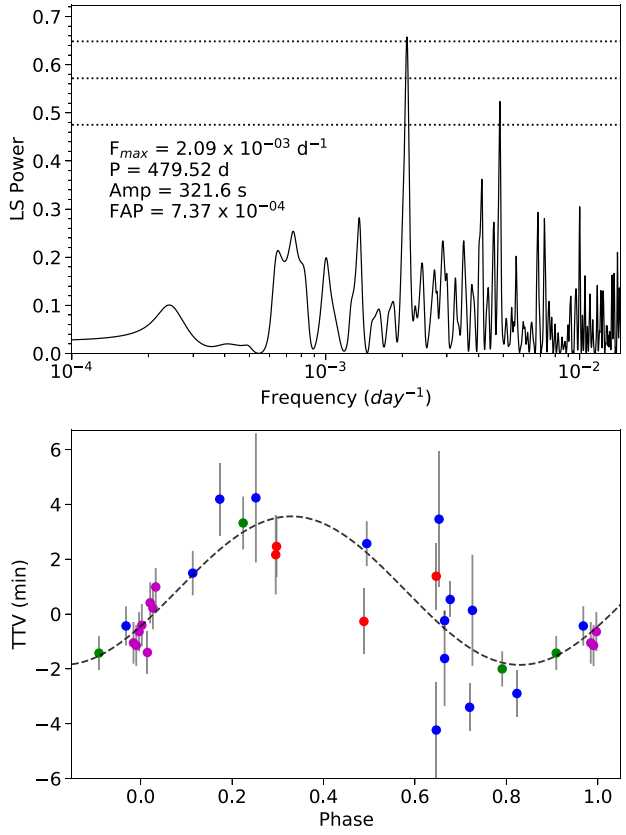

Figure 2. *Top*: Lomb–Scargle periodogram of TTV of HAT-P-13 b. The horizontal dotted lines correspond to FAPs of 0.1, 0.01, and 0.001, from bottom to top. *Bottom*: phase-folded TTV to the frequency with the highest power.

aligned. Winn et al. (2010b) speculate that hot Jupiter systems may have primordial misaligned orbits, but the tidal dissipation in the convective zones of their host stars can lead to spin–orbit alignment. Considering the relatively high effective temperature of HAT-P-16, the star should have a thin convective zone. The $T_{\rm eff}$ cut-off at which the star will have a negligible convective mass was determined at 6250 K by Pinsonneault, DePoy & Coffee (2001), while HAT-P-16's $T_{\rm eff}$ is 6158 K. Then, it should take a few Gyr for HAT-P-16 to diminish the primordial obliquity. On the other hand, using equation (2) from Adams & Laughlin (2006b) and the limits for $Q_{\rm p}$ between 10^5 and 10^6 as given by them, the tidal circularization time-scale is only 400 Myr even if the $Q_{\rm p}$ is taken to be 10^6. Assuming that the system is at least a few Gyr old based on its magnetic activity, the non-zero eccentricity may have been caused by an outer companion (Adams & Laughlin 2006a), which may have led to Kozai–Lidov oscillations. Sada & Ramón-Fox (2016) searched for TTVs, but did not detect a definitive signal because there were too few observations. Sun et al. (2023) detected orbital decay with ΔBIC = 167 and apsidal motion with ΔBIC = 317. We included light curves from several works (Buchhave et al. 2010; Ciceri et al. 2013; Pearson, Turner & Sagan 2014; Sada & Ramón-Fox 2016; Aladağ et al. 2021), adding up to a total of 62 light curves, 9 of which were eliminated; hence, we were able to form a TTV diagram covering the widest time range available for analysis. The recently published *TESS* sector ruled out the orbital decay suggested by Sun et al. (2023). We also did not detect any significant cyclic TTV, as suggested by Sun et al. (2023), that can be caused by the apsidal motion of the orbit. Although we did not detect any significant cyclic or parabolic changes, we updated the ephemeris for future observations.

3.3.6 *HAT-P-22 system*

HAT-P-22 b is a relatively dense ($M_{\rm p} = 2.147$ M$_{\rm J}$ and $R_{\rm p} = 1.080$ R$_{\rm J}$), slightly eccentric ($e = 0.0064^{+0.0080}_{-0.0046}$; Knutson et al. 2014), probably aligned (true spin–orbit angle, $\Psi = 25^{\circ} \pm 18^{\circ}$; Mancini et al. 2018) hot Jupiter discovered by Bakos et al. (2011). Linear trend in the RV residuals has been detected by Knutson et al. (2014); they suggest that this acceleration is an evidence of a presence of at least one additional body in the system. Later on, Piskorz et al. (2015) detected a spectroscopic companion with an effective temperature of 4000 K. However, this companion could not be seen in the AO observations (Ngo et al. 2015), based on which Piskorz et al. (2015) calculated the mass of the potential companion to be ∼660 M$_{\rm J}$ with a maximum separation of 33 au. If this companion is responsible for the RV trend, then it should have a face-on orbit (e.g. the inclination of the companion's orbit must be close to 0°). The companion also could have separation larger than 33 au but observed at the time when the angular separation is low, which explains the non-AO detection. Based on the mass ratio of the host star and the companion, it is possible for companion to excite the Kozai–Lidov oscillations for HAT-P-22 b from 33-au distance (see fig. 5 in Ngo et al. 2015). Moreover, the small eccentricity could be a hint for such oscillation. HAT-P-22 b is also one of the most favourable exoplanets for atmospheric characterization with TSM = 582. We included HAT-P-22 b to our list to attempt to detect TTV and/or update the ephemeris for future observations.

Ground-based photometric follow-up transit observations have been carried out by Hinse et al. (2015) and Wang et al. (2021). We used all available observations from the literature, ETD, *TESS*, and our observations, which passed our criteria (6 of them were eliminated), to form a TTV diagram of 19 data points spanning a baseline of 13 yr. We did not detect any parabolic or periodic changes, and we updated the ephemeris of the exoplanet HAT-P-22 b as a result.

3.3.7 *HAT-P-30/WASP-51 system*

HAT-P-30 b is a hot Jupiter ($M_{\rm p} = 0.711$ M$_{\rm J}$ and $R_{\rm p} = 1.340$ R$_{\rm J}$), independently discovered by Johnson et al. (2011) and Enoch et al. (2011). RV observations show that the planet has a highly oblique (i.e. misaligned) orbit but no potential perturbing companion has been detected in the system through spectral (Piskorz et al. 2015) or AO observations (Ngo et al. 2015). Enoch et al. (2011) detected a strong Lithium absorption line indicating the system is young (<1 Gyr). Therefore, it is possible that the planet has not had enough time to damp its obliquity with tidal dissipation (Winn et al. 2010a). Bai et al. (2022) detected TTV for HAT-P-30 b that could be caused by apsidal precession or additional perturbing body. We selected this system to investigate the findings of Bai et al. (2022) with the new transit observations.

We analysed a total of 48 light curves (6 of them were eliminated), including 3 *TESS* sectors and follow-up observations from the literature (Maciejewski et al. 2016a; Wang et al. 2021) and ETD observations to form the TTV diagram spanning more than 12 yr. We were able to accurately update the ephemeris, thanks to the multisector *TESS* observations. However, in contrast to Bai et al. (2022), we did not find any statistically significant TTVs.

3.3.8 HAT-P-53 system

HAT-P-53 b is a hot Jupiter ($M_p = 1.484$ M_J and $R_p = 1.318$ R_J) that orbits a Sun-like star (Hartman et al. 2015). Unfortunately, RV follow-up observations are not sufficiently precise to measure the orbital eccentricity, RM effect, or to search for additional bodies even unless they are too massive, though Hartman et al. (2015) denoted the system's RV can be precisely measured despite the relatively faint host star, thanks to its slow rotation and low surface temperature. Although the star rotates slowly, the planet moves rapidly in its orbit. Because of that, HAT-P-53 system is suggested to be a good example for tidal spin-up by Gallet (2020). As the angular momentum transferred from planet's orbit to star, star will rotate faster while planet's orbit shrinks. This effect could be observable with the TTV method if the observed time range is long enough as the amplitude of this effect increases within time. We selected this system to analyse its TTV to attempt to detect such variation.

Photometric transit follow-up observations have been carried out by Kjurkchieva et al. (2018) and Wang et al. (2021). The system has only three transit observations that cover the full transit and does not have 2-min *TESS* observations. Nevertheless, we were able to update the ephemeris of the system using the combination of ETD, literature, and 30-min *TESS* data for future observations. We did not detect any deviations from the linear ephemeris in the system in our analysis.

3.3.9 KELT-3 system

KELT-3 b is a hot Jupiter ($M_p = 1.477$ M_J and $R_p = 1.345$ R_J) orbiting a bright ($V = 9.8$ mag), late F type star discovered by Pepper et al. (2013). A faint nearby star at 3.74-arcsec angular distance was detected from direct imaging observations (Pepper et al. 2013; Wöllert & Brandner 2015). *Gaia* revealed that this neighbour is actually bound to the system at a linear distance of ∼800 au. Relatively high surface temperature and brightness of the host star make the KELT-3 system an excellent candidate for probing the atmosphere of its planet in shorter wavelengths with transit observations (e.g. Cauley, Redfield & Jensen 2017; Corrales et al. 2021) or with the occultation observations in longer wavelengths (emission spectroscopy metric, ESM = 170; Kempton et al. 2018). Despite having a bright host star, the system does not have many follow-up observations in the literature. In fact, our observation is the only one that covers a full transit. Mallonn et al. (2019) updated the ephemeris using the transit observations from ETD and observation from Pepper et al. (2013). Wang et al. (2021) observed two transits but they were not able to cover the full duration.

We have refined the ephemeris of KELT-3 b using two sectors of *TESS* observations and our observation. Based on our criteria, we eliminated the ETD and previous observations from Pepper et al. (2013). However, the *TESS* observations are relatively precise, thanks to the bright host star, enabling us to correct the ephemeris for future observations of this bright system.

3.3.10 QATAR-2 system

QATAR-2 b is a short-period ($P = 1.337$ d) hot Jupiter ($M_p = 2.487$ M_J and $R_p = 1.144$ R_J) discovered by Bryan et al. (2012). Some of the transit light curves show star-spot occultations by the planet's disc. Mancini et al. (2014) observed consecutive transits of QATAR-2 b with ground-based telescopes and they concluded that the planet's orbital plane is aligned with the stellar rotation by tracking the change in position of one star-spot. Later on, Dai et al. (2017) and Močnik, Southworth & Hellier (2017) used *Kepler* observations and also found that the planet's orbit is aligned. The findings were further confirmed by Esposito et al. (2017) based on RV observations during a transit, which revealed a symmetric RM effect in the prograde direction.

The short period and relatively high mass ratio of QATAR-2 b make it a potential target to observe an orbital decay (Dai et al. 2017 and references therein), which manifests itself as a parabolic change in the TTV diagram. The amplitude of this effect increases over time, making it detectable with ground-based observations. We observed the transit of QATAR-2 b after ∼1250 epochs later from *Kepler* observations but we did not detect statistically significant parabolic change. We also did not detect statistically significant periodic TTV in the system. Although the TTV diagram of QATAR-2 b is not well sampled, the updated ephemeris precision is the highest among the exoplanets in this study (except WASP-50 b), thanks to the ultra-precise *Kepler* data.

3.3.11 WASP-8 system

WASP-8 b is a warm Jupiter ($P = 8.1587$ d, $M_p = 2.244$ M_J, and $R_p = 1.038$ R_J), orbiting a bright ($V = 9.87$ mag) solar-like star, discovered by Queloz et al. (2010). The planet is very interesting due to its eccentric ($e = 0.3044$; Knutson et al. 2014), misaligned, and retrograde orbit ($\lambda = -143°$; Bourrier et al. 2017). In the discovery paper, the RV residuals show a linear drift, potentially caused by a companion. The system consists of a physically bound faint M type dwarf star WASP-8B, located ∼4.5 arcsec (∼440 au) away from WASP-8A (Ngo et al. 2015). Follow-up RV observations by Knutson et al. (2014) revealed that only a part of the observed slope in RV residuals can be due to the presence of WASP-8B. Instead, another planet, WASP-8 c ($P_c = 4323$ d and $M_c \sin i_c = 9.45$ M_J) was found to be responsible for the RV variation. The only photometric follow-up observations were carried out by Borsato et al. (2021) with the *CHaracterising ExOPlanet Satellite* (Benz et al. 2021) to improve the precision of ephemeris.

WASP-8 b is a promising TTV candidate and has a very high TSM (421), suitable for atmospheric observations. However, its equatorial position ($\delta \sim -35°$) and long period (hence long transit duration) make it difficult to observe its full transits. We updated the ephemeris of WASP-8 b with three sectors of *TESS* observations and two light curves from previously published observations. This updated ephemeris will be useful for future ground- and space-based observations of the system.

3.3.12 WASP-44 system

WASP-44 b is a hot Jupiter ($M_p = 0.889$ M_J and $R_p = 1.14$ R_J) discovered by Anderson et al. (2012). Mancini et al. (2013) found that the radius of the planet is smaller by 10 per cent than first measured and there is no extreme radius variation in the optical wavelengths from multiband photometry. However, Turner et al. (2016) reported that the radius of the planet is 1.4σ larger in the near-ultraviolet. After ∼6.5 yr, Addison et al. (2019) observed a transit and updated the ephemeris. Similar to the HAT-P-30 system, WASP-44 system is also exposed to tidal spin-up (Gallet 2020). Similar study has been carried out by Brown (2014) and isochrone age was found to be significantly older than gyrochronological age. The angular momentum transfer from planet's orbit to rotation of the star could manifest itself as orbital decay in TTV diagram. We selected this system to attempt to detect such variation.

We analysed the follow-up transit observations mentioned above, along with our own observations, and *TESS* and ETD data, to update the ephemeris. However, we did not find any evident periodic or secular TTVs in its timing data.

3.3.13 WASP-50 system

WASP-50 b is a hot Jupiter ($M_p = 1.468$ M_J and $R_p = 1.53$ R_J), discovered by Gillon et al. (2011) revolving on a circular orbit (Bonomo et al. 2017). Follow-up photometric transit observations were carried out by Tregloan-Reed & Southworth (2013), Sada et al. (2012), and Sada (2018) to update the ephemeris or increase the precision of its transit parameters. Gillon et al. (2011) measured the rotation period of WASP-50 from two seasons of WASP photometry as 16.3 ± 0.5 d; however, Canto Martins et al. (2020) found this value to be only 5.488 d from *TESS* Sector 4 light curve. We performed a preliminary analysis of the Sector 31 PDCSAP_FLUX of *TESS* and confirmed the finding by Canto Martins et al. (2020). The measured $\log R'_{HK}$ and P_{rot} values by Gillon et al. (2011) are in excellent agreement with each other comparing to the empirical values calculated using the P_{rot}–$\log R'_{HK}$ relation presented by Suárez Mascareño et al. (2015). Moreover, a rotation rate of 5.488 d indicates a very young age (∼80 Myr; Barnes 2007); however, according to the lithium abundance, the system should be at least 0.6 ± 0.2 Gyr old (Gillon et al. 2011). If the true rotation period is 5.488 d, then the lack of lithium suggests that the star could be a good example of tidal spin-up (e.g. Gallet 2020). Tejada Arevalo, Winn & Anderson (2021) have suggested that even after orbital circularization, the planet's orbit may shrink by transferring angular momentum to its host star and causing its rotation rate to increase. We selected this system to observe such effect via TTV method as it should manifest itself as orbital decay.

We analysed 45 light curves (9 of them were eliminated) spanning 10 yr of best observations available. We did not detect any parabolic TTV but the frequency analysis peaked at 34.45 d with an FAP of 2 per cent. The amplitude of this periodic variation is 57 s, which is compatible with our average mid-transit uncertainty. As a result, our findings are inconclusive. Further precise observations are required to confirm this hint of a periodic TTV.

3.3.14 WASP-77 system

WASP-77A b is a short-period ($P = 1.36$ d) hot Jupiter ($M_p = 1.76$ M_J and $R_p = 1.21$ R_J) revolving around a G8 V-type, bright ($V = 10.12$ mag), wide binary with the component WASP-77B at a projected angular distance of ∼3.5 arcsec (Maxted et al. 2013). Photometric follow-up transit observations that confirmed the transit parameters of the discovery paper were carried out by Turner et al. (2016) and Cortés-Zuleta et al. (2020). The planet has relatively high TSM and ESM (ESM = 333 and TSM = 770) and its wide companion (WASP-77B) can be used as a comparison star, making it favourable for atmospheric observations via transmission or emission spectroscopy from the ground-based (Line et al. 2021; Reggiani et al. 2022) or space-borne observations (Mansfield et al. 2022). Gallet (2020) suggested that the host star might have been affected by tidal spin-up by its planet WASP-77 b.

Cortés-Zuleta et al. (2020) performed a TTV analysis for WASP-77 b in a similar way within this work. We added additional transit light curves from *TESS* Sector 31, our observations, and the newly available light curves from ETD. As a result, we were able to update the ephemeris with increased precision, thanks to transit light curves covering a longer baseline. As in Cortés-Zuleta et al. (2020), we found no significant secular or periodic TTVs.

3.3.15 WASP-93 system

WASP-93 b is a hot Jupiter ($M_p = 1.47$ M_J and $R_p = 1.597$ R_J) orbiting a fast-rotating ($v \sin i = 37 \pm 3$ km s^{-1}) F4 V star discovered by Hay et al. (2016). RM observations were attempted twice by Hay et al. (2016); however, the first observation was unable to cover the transit due to ephemeris uncertainty, and the combination of the first and second attempts resulted in inconclusive results due to insufficient RV precision. Gajdoš et al. (2019) searched for TTVs in the system using only ETD observations and they did not observe any significant deviation from linear ephemeris. Although WASP-93 b has relatively high TSM and ESM, *TESS* observations do not show significant phase modulations or an occultation signal (Wong et al. 2021).

TESS observed WASP-93 during sectors 17, 57, and 58 but, unfortunately, the object was too close to the edge of the camera in Sector 58 observations; hence, we were unable to use it. We observed seven transits of WASP-93 b and used available observations in the literature and ETD to update its ephemeris. The RM observations by Hay et al. (2016) show the hint of a retrograde orbit if the transit ephemeris arrived earlier by ∼35 min. The timing difference between our ephemeris and the ephemeris from Hay et al. (2016) is only -46 ± 48 s at the time of the second RM observations. Therefore, we rule out the early transit-retrograde orbit scenario even if the two independent RM observations agree with each other (see fig. 8 in Hay et al. 2016). We also did not detect any secular or periodic TTV signal.

3.3.16 XO-2N system

XO-2N b is a hot Jupiter ($M_p = 0.57$ M_J and $R_p = 0.98$ R_J) orbiting around a metal-rich, [M/H] $= 0.44 \pm 0.02$ dex, wide binary component XO-2N in an aligned orbit (Narita et al. 2011) discovered by Burke et al. (2007). A binary companion, XO-2S, which is also a metal-rich star, resides ∼30 arcsec away from XO-2N and has at least two planets discovered with RV observations (Desidera et al. 2014). The visual binary components have similar effective temperatures; thus, XO-2S is a great comparison star for transmission spectroscopy of XO-2N b (e.g. Crouzet et al. 2012; Sing et al. 2012). With additional RV observations, Knutson et al. (2014) detected that the RV residuals show a linear trend within time, possibly caused by an outer companion. Later on, Damasso et al. (2015) revealed that the linear RV residuals are actually only a part of the curve in RV, possibly caused by an outer companion XO-2N c or by stellar activity.

We obtained the transit light curves from several works (Burke et al. 2007; Fernandez et al. 2009; Kundurthy et al. 2011; Damasso et al. 2015; Maciejewski et al. 2018; Wang et al. 2021), 3 sectors of observation (20, 47, and 60) from *TESS*, 13 from amateur astronomers, and our 3 new observations to form the TTV diagram with a total of 42 light curves, spanning almost 16 yr. Our analyses indicated that the parabolic ephemeris fits the data better than linear with the ΔBIC of 42.98 and ΔAIC of 45.15, suggesting that the orbit of XO-2 b is decaying with a rate of -12.95 ± 1.85 ms yr^{-1} (Fig. 3). The parabolic ephemeris is as follows:

$$T = 2458\,843.218\,212(92) + 2.615\,858\,62(17)\,E - 4.7(8) \times 10^{-10}\,E^2. \quad (1)$$

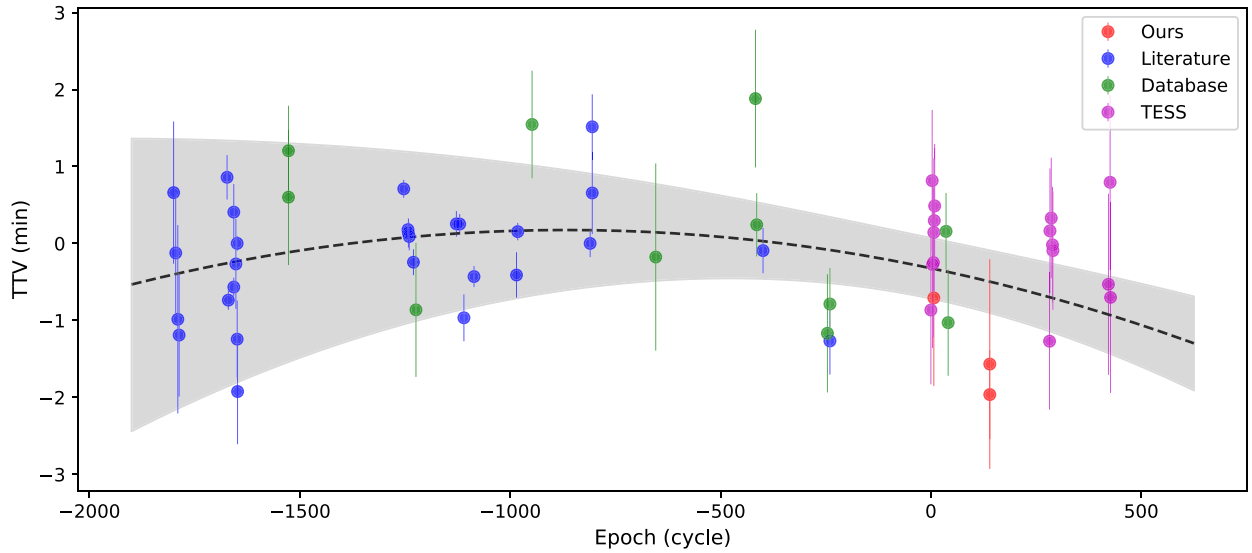

Figure 3. Quadratic TTV model of XO-2N b (black dashed line with 3σ uncertainty shown in grey shaded region). The linear term was subtracted for display purposes.

Although the parabolic ephemeris is statistically significant, it does not agree well with the latest *TESS* observations (sectors 47 and 60). *TESS* will observe the XO-2N system during cycle 6 of its mission. However, the wide binary component is only ∼30 arcsec away, and a *TESS* pixel has a 21-arcsec field of view. This may add extra red and white noise because the light from XO-2S blends into the aperture selected for XO-2N. Therefore, ground-based observations could be a better option for confirming or discarding the parabolic trend.

4 DISCUSSION

We constructed the TTV diagrams of 16 exoplanets consisting of the most precise and complete light curves with the longest time span for each of the planets in our sample (Fig. 1). This allowed us to increase the precision of the orbital period and the accuracy of the ephemeris information for future follow-up observations. Based on the ephemeris information given in Table 3, the uncertainty on the predicted ephemeris will provide transit timings with a precision below 5 min with an average of 1.8 min until 2070 for all the systems except for XO-2N and HAT-P-13 where we detect deviation from the linear ephemeris.

We detect that a decrease in the orbital period of XO-2N b may have been caused by several events if it is real. As discussed by Vissapragada et al. (2022), such a decrease can be observed if the system is accelerating towards us, making the transits observed earlier than expected. In that case, the RV residuals should have a slope of $-0.05\,\mathrm{m\,s^{-1}\,d^{-1}}$ ($\dot{v} = c\dot{P}/P$; Vissapragada et al. 2022) but Damasso et al. (2015) reported this value as $+0.0017\,\mathrm{m\,s^{-1}\,d^{-1}}$. Damasso et al. (2015) also reported that the eccentricity of the planet is consistent with zero. Therefore, we did not consider a scenario based on precession. The RV residuals show a parabolic variation that can be caused by a long-period outer companion. This companion may be causing LiTE and changing the orbital period of XO-2 b within a longer time interval; thus, the parabolic TTV could be a part of this periodic variation. We neglect this scenario also because Damasso et al. (2015) showed that the parabolic RV variation is due to magnetic activity. Even if the magnetic activity was not the reason for the RV residuals, the phases of LiTE and long-term parabolic RV change do not match.

We detect a cyclic variation in the period of HAT-P-13 b, which has a semi-amplitude of 160.8 s and 479.52-d periodicity. This variation could be caused by the known outer companion of the system, HAT-P-13 c ($P = 445.82 \pm 0.11$ d and $M_\mathrm{p} \sin i = 14.61^{+0.46}_{-0.48}$ M$_\mathrm{J}$; Knutson et al. 2014). However, in order to cause such a high-amplitude TTV, the orbital inclination of HAT-P-13 c needs to be ∼2°, which translates into a mass of ∼0.4 M$_\odot$ using the $M_\mathrm{p} \sin i$ value. Piskorz et al. (2015) detected another star in the spectrum of HAT-P-13 that has an effective temperature of 3900^{+300}_{-350} K ($M_\mathrm{companion} = 0.6^{+0.086}_{-0.179}$ M$_\odot$). Piskorz et al. (2015) discussed whether HAT-P-13 d, detected by linear drift in the RV residuals, is that spectral companion. However, in that case, the inclination of the planet d should be ∼5°, which could lead to Kozai–Lidov oscillations and make the orbit of HAT-P-13 b misaligned (Winn et al. 2010a). Our TTV analysis suggests that the observed spectral companion could be HAT-P-13 c instead. This could explain the non-AO detection by Ngo et al. (2015) due to short angular separation. However, such a close companion would have catastrophic effects on the system stability aside from making the orbit of HAT-P-13 b misaligned.

Nevertheless, in order to assess the time-scale of any potential orbital instability of the planet c with an orbital inclination of 2°, we run an *N*-body simulation by using REBOUND code (Rein & Liu 2012), with 15th-order integrator to simulate gravitational dynamics (IAS15) (Rein & Spiegel 2015) integrator. We used the masses and orbital parameters of the planets b and c derived from Winn et al. (2010a). We stress that we did not include the potential additional planet (planet d in Knutson et al. 2014), since the orbital parameters and mass of this putative object are currently unknown. Results of our simulation show that the system becomes unstable of the order of 30 000 yr. Therefore, we think that the amplitude of the detected TTV signal in our analysis might have been overestimated due to the high scatter caused by correlated noise in the transit light curves.

We do not find any statistically significant periodicities in our timing analysis of any other system. However, we simulated the WASP-8 system in a same way as we did for HAT-P-13 and we found that the TTV due to WASP-8 c should be observable. We assumed that the transiting planet WASP-4 b is coplanar with the RV

planet WASP-8 c. Using the absolute and orbital parameters from Queloz et al. (2010) and Knutson et al. (2014), we found that the full TTV amplitude of WASP-8 b should be ∼40 s due to LiTE and ∼2 s due to gravitational interaction. The typical mid-transit measurement error of *TESS* data for this system is about 20 s, so the TTV of this system can be detected with light curves that have similar precision as *TESS*. We could not detect this signal due to poor phase coverage.

4.1 Discussion on tidal quality factors

Although we do not have any observational data on the rotation rates of the exoplanets in our sample, the rotational periods of their hosts are all longer compared to their orbital periods. The energy raised in those tidal interactions can be dissipated in the convective envelope of their host stars, transferring angular momentum from the planet to the star that would cause the star to spin-up while the planet to fall-in (Counselman 1973; Rasio et al. 1996; Essick & Weinberg 2016; Harre et al. 2023; Weinberg et al. 2024). In addition to this equilibrium tide, dynamical tide excites internal gravity waves, which dissipate the energy through also the secondary waves it generates via wave–wave interactions (Barker & Ogilvie 2010; Ivanov, Papaloizou & Chernov 2013; Barker 2020). This latter mechanism is especially dominant in a system with a solar-type host and a hot Jupiter-type planet (Essick & Weinberg 2016; Weinberg et al. 2024).

If we assume the planetary mass to be constant, then the rate of change in the orbital period can be related to the so-called reduced tidal quality factor of the host star by the constant phase lag model of Goldreich & Soter (1966) defined as

$$Q'_\star = -\frac{27\pi}{2}\left(\frac{M_\mathrm{p}}{M_\star}\right)\left(\frac{R_\star}{a}\right)^5\frac{1}{\dot{P}}, \tag{2}$$

where M_p is the mass of the planet, $M_\star$ and $R_\star$ are the mass and the radius of the host star, respectively, and a is the semimajor axis of the planet's orbit. The rate of orbital decay, $\dot{P}$, is derived from the timing analysis, which is twice the value of the quadratic coefficient of the best-fitting parabola. If that best-fitting model is not found to be statistically superior to the linear model, then an orbital decay cannot be argued and the quadratic coefficient can only be used to derive a lower limit for the reduced tidal quality factor, which is the case for all systems in our sample except XO-2N. We derived these limits based on the fundamental parameters of the objects in our sample, which we provide in Table 4 together with ΔAIC and ΔBIC values, indicating the statistical significance of the quadratic model in each of the cases. Positive values for both statistics hint that the quadratic model should be favoured.

XO-2N b is not one of the prime candidates for orbital decay due to tidal interactions with its host star because it is not a particularly big planet. Although its solar-like host star should have a convective envelope to dissipate the tidal energy, its reduced tidal quality factor should be larger than 550 as derived from the rate of observed period decrease when it is compared with other host stars with similar spectral types and evolutionary history. Infall time calculated from the same rate is $P/\dot{P} \approx 17.45$ Myr, which is too short compared to age of the system. *TESS* observations do not follow the orbital decay model found to be statistically superior to the linear model. However, the precision of *TESS* observations of XO-2N is lower than that achieved for the stars with similar magnitudes. This is because the wide binary component XO-2S is only ∼30 arcsec away from the XO-2N, blending its flux in the *TESS* aperture, adding extra noise and diluting the transit depth, resulting in high scatter on the TTV diagram. Because of this reason, we encourage observations of the transit of XO-2N b with ground-based telescopes in high angular resolution in the future to confirm the orbital decay scenario, which we find unlikely at the moment.

ACKNOWLEDGEMENTS

We gratefully acknowledge the support by the Scientific and Technological Research Council of Türkiye (TÜBİTAK) with project 118F042. We thank TÜBİTAK for the partial support in using the T100 telescope with the project numbers 12CT100-378, 16BT100-1034, 17BT100-1196, and 19AT00-1472. The data in this study were obtained with the T80 telescope at the Ankara University Astronomy and Space Sciences Research and Application Center (Kreiken Observatory) with project number 22B.T80.10. We thank the observers in AUKR, UZAYMER, ATASAM, TUG, observatories, and all the observers around the world who kindly shared their data with us. This research has made use of data obtained using the ATA50 telescope and the CCD attached to it, operated by Atatürk University Astrophysics Research and Application Center (ATASAM). Funding for the ATA50 telescope and the attached CCD has been provided by Atatürk University (P. No. BAP-2010/40) and Erciyes University (P. No. FBA-11-3283) through Scientific Research Projects Coordination Units (BAP), respectively. This study was funded by the Scientific Research Projects Coordination Unit of Istanbul University (P. No. FBA-2022-39121). Authors from Bilkent University thank the internship programme of Ankara University Kreiken Observatory (AUKR). We thank all the observers who report their observations to ETD and AXA open data bases. LM acknowledges support from the MIUR-PRIN project No. 2022J4H55R. This works is based on observations performed at the Centro Astronómico Hispano en Andalucía (CAHA) at Calar Alto, operated jointly by Junta de Andalucía and Consejo Superior de Investigaciones Científicas (IAA-CSIC). This work includes data collected with the *TESS* mission, obtained from the MAST data archive at the Space Telescope Science Institute (STScI). Funding for the *TESS* mission is provided by the NASA Explorer Program. STScI is operated by the Association of Universities for Research in Astronomy, Inc., under NASA contract NAS 5–26555. We acknowledge the use of public *TESS* data from pipelines at the *TESS* Science Office and at the *TESS* SPOC. Resources supporting this work were provided by the NASA High-End Computing (HEC) Program through the NASA Advanced Supercomputing (NAS) Division at Ames Research Center for the production of the SPOC data products. This paper includes data collected by the *Kepler* mission and obtained from the MAST data archive at the STScI. Funding for the *Kepler* mission is provided by the NASA Science Mission Directorate. This work has made use of data from the European Space Agency (ESA) mission *Gaia* (https://www.cosmos.esa.int/gaia), processed by the *Gaia* Data Processing and Analysis Consortium (DPAC; https://www.cosmos.esa.int/web/gaia/dpac/consortium). Funding for the DPAC has been provided by national institutions, in particular, the institutions participating in the *Gaia* Multilateral Agreement.

DATA AVAILABILITY

Some of the light curves to derive mid-transit times were downloaded from ETD at http://var2.astro.cz/ETD/. All other light curves appearing for the first time in this article are presented as online material.

Mid-transit times derived from our own light curves as well as those of other observers are presented as online data sets too.

REFERENCES

Adams F. C., Laughlin G., 2006a, ApJ, 649, 992
Adams F. C., Laughlin G., 2006b, ApJ, 649, 1004
Addison B. et al., 2019, PASP, 131, 115003
Aladağ Y., Akyüz A., Bastürk Ö., Aksaker N., Esmer E. M., Yalçınkaya S., 2021, Turk. J. Astron. Astrophys., 2, 28
Anderson D. R. et al., 2012, MNRAS, 422, 1988
Angerhausen D. et al., 2017, A&A, 608, A120
Arcangeli J., Désert J. M., Parmentier V., Tsai S. M., Stevenson K. B., 2021, A&A, 646, A94
Astropy Collaboration, 2013, A&A, 558, A33
Astropy Collaboration, 2018, AJ, 156, 123
Bai L., Gu S., Wang X., Sun L., Kwok C.-T., Hui H.-K., 2022, AJ, 163, 208
Bakos G. Á. et al., 2007, ApJ, 656, 552
Bakos G. Á. et al., 2009a, ApJ, 696, 1950
Bakos G. Á. et al., 2009b, ApJ, 707, 446
Bakos G. Á. et al., 2011, ApJ, 742, 116
Barker A. J., 2020, MNRAS, 498, 2270
Barker A. J., Ogilvie G. I., 2010, MNRAS, 404, 1849
Barnes S. A., 2007, ApJ, 669, 1167
Baştürk Ö. et al., 2022, MNRAS, 512, 2062
Benz W. et al., 2021, Exp. Astron., 51, 109
Bonfanti A., Ortolani S., Piotto G., Nascimbeni V., 2015, A&A, 575, A18
Bonomo A. S. et al., 2017, A&A, 602, A107
Borsato L. et al., 2021, MNRAS, 506, 3810
Bourrier V., Cegla H. M., Lovis C., Wyttenbach A., 2017, A&A, 599, A33
Brown D. J. A., 2014, MNRAS, 442, 1844
Bryan M. L. et al., 2012, ApJ, 750, 84
Buchhave L. A. et al., 2010, ApJ, 720, 1118
Burke C. J. et al., 2007, ApJ, 671, 2115
Cáceres C. et al., 2014, A&A, 565, A7
Canto Martins B. L. et al., 2020, ApJS, 250, 20
Cauley P. W., Redfield S., Jensen A. G., 2017, AJ, 153, 81
Charbonneau D., Brown T. M., Latham D. W., Mayor M., 2000, ApJ, 529, L45
Charbonneau D. et al., 2009, Nature, 462, 891
Ciceri S. et al., 2013, A&A, 557, A30
Claret A., Bloemen S., 2011, A&A, 529, A75
Cloutier R., Charbonneau D., Deming D., Bonfils X., Astudillo-Defru N., 2021, AJ, 162, 174
Collins K. A., Kielkopf J. F., Stassun K. G., Hessman F. V., 2017, AJ, 153, 77
Corrales L., Ravi S., King G. W., May E., Rauscher E., Reynolds M., 2021, AJ, 162, 287
Cortés-Zuleta P., Rojo P., Wang S., Hinse T. C., Hoyer S., Sanhueza B., Correa-Amaro P., Albornoz J., 2020, A&A, 636, A98
Counselman C. C., III, 1973, ApJ, 180, 307
Crouzet N., McCullough P. R., Burke C., Long D., 2012, ApJ, 761, 7
Dai F., Winn J. N., Yu L., Albrecht S., 2017, AJ, 153, 40
Damasso M. et al., 2015, A&A, 575, A111
de Mooij E. J. W. et al., 2012, A&A, 538, A46
Desidera S. et al., 2014, A&A, 567, L6
Eastman J., Gaudi B. S., Agol E., 2013, PASP, 125, 83
Enoch B. et al., 2011, AJ, 142, 86
Esposito M. et al., 2017, A&A, 601, A53
Essick R., Weinberg N. N., 2016, ApJ, 816, 18
Fernandez J. M., Holman M. J., Winn J. N., Torres G., Shporer A., Mazeh T., Esquerdo G. A., Everett M. E., 2009, AJ, 137, 4911
Foreman-Mackey D., Hogg D. W., Lang D., Goodman J., 2013, PASP, 125, 306
Fulton B. J., Shporer A., Winn J. N., Holman M. J., Pál A., Gazak J. Z., 2011b, AJ, 142, 84
Gajdoš P. et al., 2019, MNRAS, 485, 3580
Gallet F., 2020, A&A, 641, A38
Gao P. et al., 2023, ApJ, 951, 96
Gillon M., Pont F., Moutou C., Bouchy F., Courbin F., Sohy S., Magain P., 2006, A&A, 459, 249
Gillon M. et al., 2011, A&A, 533, A88
Gillon M. et al., 2014, A&A, 563, A21
Gillon M. et al., 2017, Nature, 542, 456
Giménez A., Bastero M., 1995, Ap&SS, 226, 99
Goldreich P., Soter S., 1966, Icarus, 5, 375
Harpsøe K. B. W. et al., 2013, A&A, 549, A10
Harre J. V. et al., 2023, A&A, 669, A124
Hartman J. D. et al., 2015, AJ, 150, 168
Hay K. L. et al., 2016, MNRAS, 463, 3276
Hinse T. C., Han W., Yoon J.-N., Lee C.-U., Kim Y.-G., Kim C.-H., 2015, J. Astron. Space Sci., 32, 21
Howell S. B. et al., 2014, PASP, 126, 398
Ivanov P. B., Papaloizou J. C. B., Chernov S. V., 2013, MNRAS, 432, 2339
Jenkins J. M. et al., 2016, in Chiozzi G., Guzman J. C., eds, Proc. SPIE Conf. Ser. Vol. 9913, Software and Cyberinfrastructure for Astronomy IV. SPIE, Bellingham, p. 99133E

Johnson J. A. et al., 2008, ApJ, 686, 649
Johnson J. A. et al., 2011, ApJ, 735, 24
Kempton E. M. R. et al., 2018, PASP, 130, 114401
Kjurkchieva D., Petrov N., Ibryamov S., Nikolov G., Popov V., 2018, Serb. Astron. J., 196, 15
Knutson H. A., Howard A. W., Isaacson H., 2010, ApJ, 720, 1569
Knutson H. A. et al., 2014, ApJ, 785, 126
Kundurthy P., Agol E., Becker A. C., Barnes R., Williams B., Mukadam A., 2011, ApJ, 731, 123
Lampón M. et al., 2023, A&A, 673, A140
Lightkurve Collaboration, 2018, Astrophysics Source Code Library, record ascl:1812.013
Line M. R. et al., 2021, Nature, 598, 580
Maciejewski G. et al., 2016a, Acta Astron., 66, 55
Maciejewski G. et al., 2016b, A&A, 588, L6
Maciejewski G., Stangret M., Ohlert J., Basaran C. S., Maciejczak J., Puciata-Mroczynska M., Boulanger E., 2018, Inf. Bull. Var. Stars, 6243, 1
Maguire C., Gibson N. P., Nugroho S. K., Ramkumar S., Fortune M., Merritt S. R., de Mooij E., 2023, MNRAS, 519, 1030
Mallonn M. et al., 2018, A&A, 614, A35
Mallonn M. et al., 2019, A&A, 622, A81
Mancini L. et al., 2013, MNRAS, 430, 2932
Mancini L. et al., 2014, MNRAS, 443, 2391
Mancini L. et al., 2015, A&A, 579, A136
Mancini L. et al., 2017, MNRAS, 465, 843
Mancini L. et al., 2018, A&A, 613, A41
Mancini L. et al., 2022, A&A, 664, A162
Mansfield M. et al., 2022, AJ, 163, 261
Maxted P. F. L. et al., 2013, PASP, 125, 48
Ment K., Fischer D. A., Bakos G., Howard A. W., Isaacson H., 2018, AJ, 156, 213
Močnik T., Southworth J., Hellier C., 2017, MNRAS, 471, 394
Montalto M., Iro N., Santos N. C., Desidera S., Martins J. H. C., Figueira P., Alonso R., 2015, ApJ, 811, 55
Moutou C. et al., 2011, A&A, 533, A113
Narita N., Hirano T., Sato B., Harakawa H., Fukui A., Aoki W., Tamura M., 2011, PASJ, 63, L67
Narita N. et al., 2013, ApJ, 773, 144
Nascimbeni V., Piotto G., Bedin L. R., Damasso M., Malavolta L., Borsato L., 2011, A&A, 532, A24
Nascimbeni V. et al., 2015, A&A, 579, A113
Nelder J. A., Mead R., 1965, Comput. J., 7, 308
Ngo H. et al., 2015, ApJ, 800, 138
Ngo H. et al., 2016, ApJ, 827, 8
Noyes R. W., Hartmann L. W., Baliunas S. L., Duncan D. K., Vaughan A. H., 1984, ApJ, 279, 763
Orell-Miquel J. et al., 2022, A&A, 659, A55
Pál A., Sárneczky K., Szabó G. M., Szing A., Kiss L. L., Mező G., Regály Z., 2011, MNRAS, 413, L43
Parviainen H., Aigrain S., Thatte N., Barstow J. K., Evans T. M., Gibson N., 2015, MNRAS, 453, 3875
Patra K. C., Winn J. N., Holman M. J., Yu L., Deming D., Dai F., 2017, AJ, 154, 4
Pearson K. A., Turner J. D., Sagan T. G., 2014, New Astron., 27, 102
Pepper J. et al., 2013, ApJ, 773, 64
Pinsonneault M. H., DePoy D. L., Coffee M., 2001, ApJ, 556, L59
Piskorz D., Knutson H. A., Ngo H., Muirhead P. S., Batygin K., Crepp J. R., Hinkley S., Morton T. D., 2015, ApJ, 814, 148
Stanislav P., Brát L. Pejcha O. , 2010, New Astron., 15, 297
Pont F., Zucker S., Queloz D., 2006, MNRAS, 373, 231
Queloz D. et al., 2010, A&A, 517, L1
Rackham B. et al., 2017, ApJ, 834, 151
Raftery A. E., 1995, Sociol. Methodol., 25, 111
Rasio F. A., Tout C. A., Lubow S. H., Livio M., 1996, ApJ, 470, 1187
Reggiani H., Schlaufman K. C., Healy B. F., Lothringer J. D., Sing D. K., 2022, AJ, 163, 159
Rein H., Liu S. F., 2012, A&A, 537, A128
Rein H., Spiegel D. S., 2015, MNRAS, 446, 1424
Ricker G. R. et al., 2015, J. Astron. Telesc. Instrum. Syst., 1, 014003
Ridden-Harper A., Turner J. D., Jayawardhana R., 2020, AJ, 160, 249
Sada P. V., 2018, in AAS/Division for Planetary Sciences Meeting Abstracts #50. p. 413.01
Sada P. V. et al., 2012, PASP, 124, 212
Sada P. V., Ramón-Fox F. G., 2016, PASP, 128, 024402
Sing D. K. et al., 2012, MNRAS, 426, 1663
Southworth J. et al., 2009, MNRAS, 396, 1023
Southworth J., Bruni I., Mancini L., Gregorio J., 2012, MNRAS, 420, 2580
Spake J. J. et al., 2022, ApJ, 939, L11
Suárez Mascareño A., Rebolo R., González Hernández J. I., Esposito M., 2015, MNRAS, 452, 2745
Sun L., Gu S., Wang X., Bai L., Schmitt J. H. M. M., Perdelwitz V., Ioannidis P., 2023, MNRAS, 520, 1642
Szabó G. M. et al., 2010, A&A, 523, A84
Tejada Arevalo R. A., Winn J. N., Anderson K. R., 2021, ApJ, 919, 138
Tregloan-Reed J., Southworth J., 2013, MNRAS, 431, 966
Trifonov T. et al., 2021, AJ, 162, 283
Turner J. D. et al., 2016, MNRAS, 459, 789
VanderPlas J. T., 2018, ApJS, 236, 16
Vissapragada S. et al., 2022, ApJ, 941, L31
Wakeford H. R. et al., 2013, MNRAS, 435, 3481
Wang X.-b., Gu S.-h., Collier Cameron A., Wang Y.-b., Hui H.-K., Kwok C.-T., Yeung B., Leung K.-C., 2014, AJ, 147, 92
Wang X.-Y. et al., 2021, ApJS, 255, 15
Weinberg N. N., Davachi N., Essick R., Yu H., Arras P., Belland B., 2024, ApJ, 960, 50
West R. G. et al., 2009, A&A, 502, 395
Winn J. N. et al., 2007, AJ, 134, 1707
Winn J. N. et al., 2008, ApJ, 683, 1076
Winn J. N. et al., 2010a, ApJ, 718, 575
Winn J. N., Fabrycky D., Albrecht S., Johnson J. A., 2010b, ApJ, 718, L145
Wong I. et al., 2021, AJ, 162, 127
Wöllert M., Brandner W., 2015, A&A, 579, A129
Yalçınkaya S. et al., 2021, Acta Astron., 71, 223

SUPPORTING INFORMATION

Supplementary data are available at *MNRAS* online.

supplementary_material_online.zip

Please note: Oxford University Press is not responsible for the content or functionality of any supporting materials supplied by the authors. Any queries (other than missing material) should be directed to the corresponding author for the article.

APPENDIX A: LIGHT CURVES

We provide our own light curves (black data points) and EXOFAST models (red continuous curves) in Figs A1–A14.

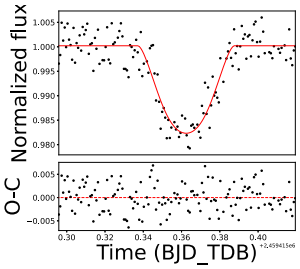

(a) T100 2021/07/19*

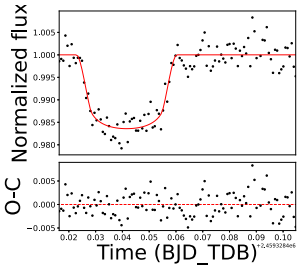

(b) T100 2021/04/23

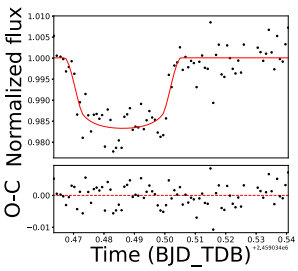

(c) T100 2020/07/03

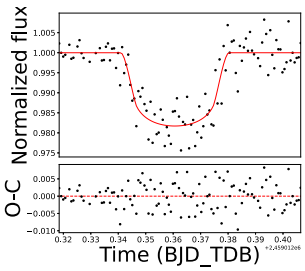

(d) T100 2020/06/11

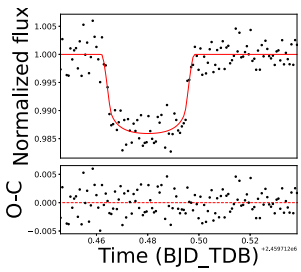

(e) T80 2020/05/12

Figure A1. GJ 1214 b light curves. Data points are shown with dots, while the continuous curve is for the EXOFAST model in all the light curves presented in this section. The ones that were eliminated based on our quantitative light-curve selection criteria, therefore not used in timing analyses, are marked with asterisks.

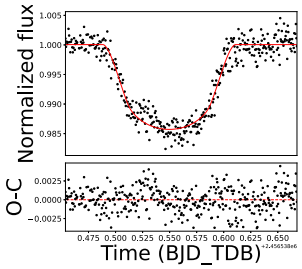

(a) CAHA 2013/09/02 b filter

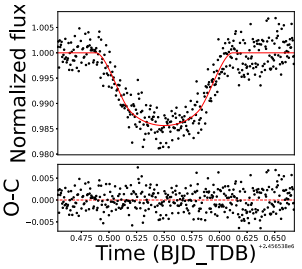

(b) CAHA 2013/09/02 u filter

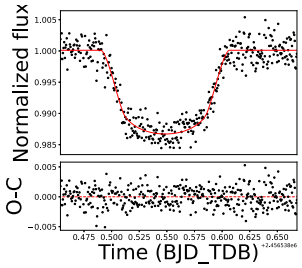

(c) CAHA 2013/09/02 y filter

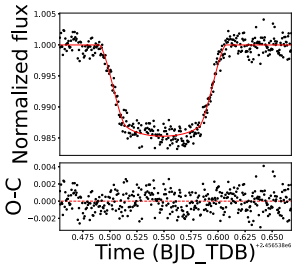

(d) CAHA 2013/09/02 z filter

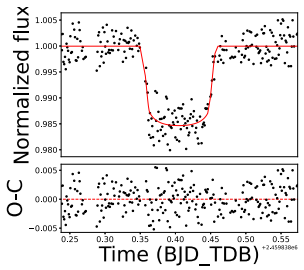

(e) ATA50 2022/09/15

Figure A2. HAT-P-1 b light curves.

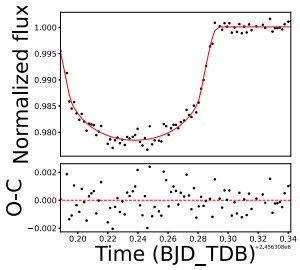

(a) T100 2013/01/15

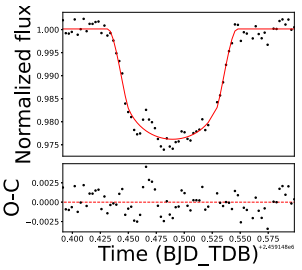

(b) T100 2020/10/25*

Figure A3. HAT-P-10 b light curves.

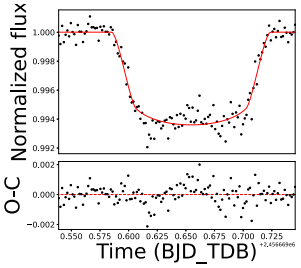

(a) CAHA 2014/01/12

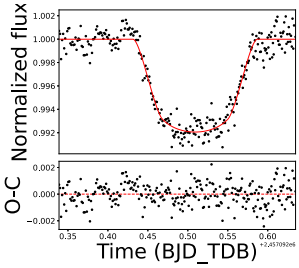

(b) CAHA 2015/03/10

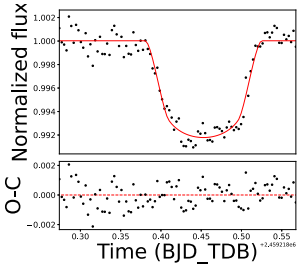

(c) T100 2021/01/03

Figure A4. HAT-P-13 b light curves.

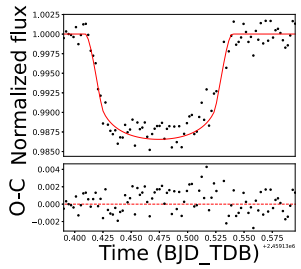

(a) ATA50 2020/10/07

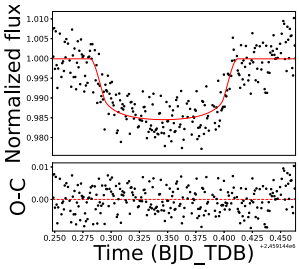

(b) UT50 2020/10/21*

Figure A5. HAT-P-16 b light curves.

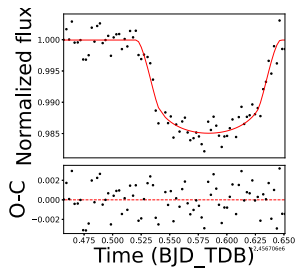

(a) T100 2014/02/17

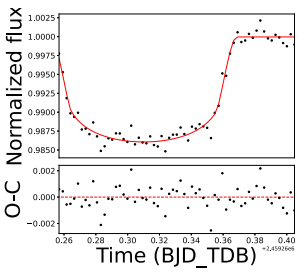

(b) T100 2021/02/14

Figure A6. HAT-P-22 b light curves.

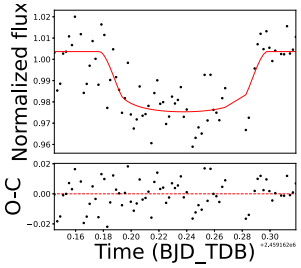

(a) ATA50 2020/11/08*

Figure A7. HAT-P-53 b light curves.

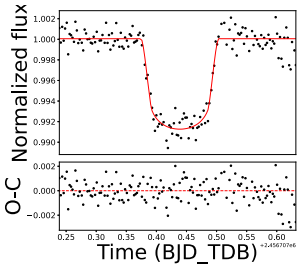

(a) T100 2014/02/18

Figure A8. KELT-3 b light curves.

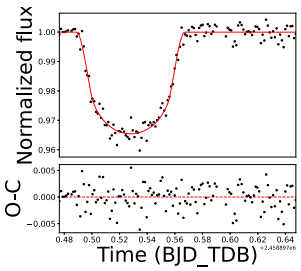

(a) T100 2019/02/17

Figure A9. QATAR-2 b light curves.

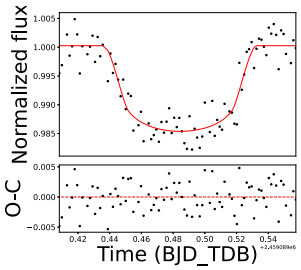

(a) T100 2020/08/27

Figure A10. WASP-44 b light curves.

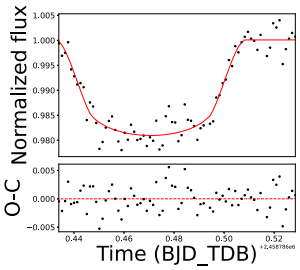

(a) T100 2019/10/29

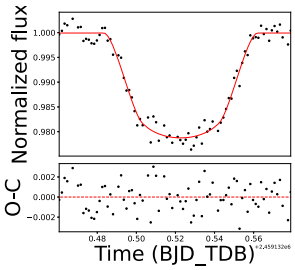

(b) T100 2020/10/09

Figure A11. WASP-50 b light curves.

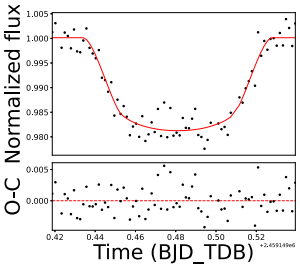

(a) ATA50 2020/10/26

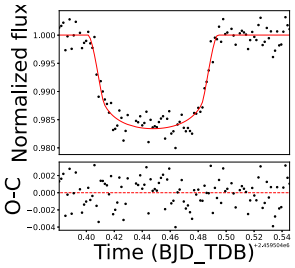

(b) ATA50 2021/10/16

Figure A12. WASP-77 b light curves.

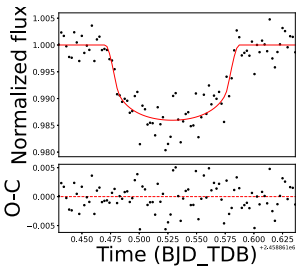

(a) T100 2020/01/12

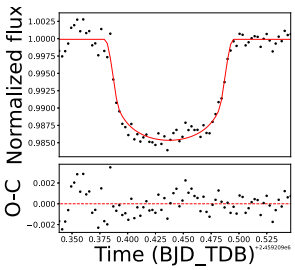

(b) T100 2020/12/25

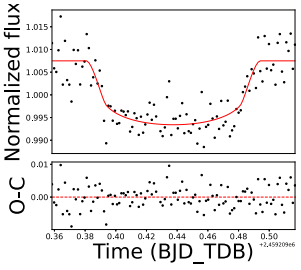

(c) T100 2020/12/25

Figure A13. XO-2 b light curves.

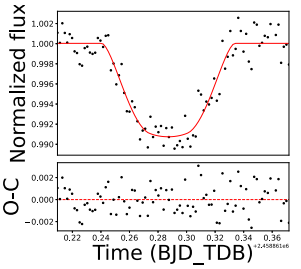

(a) T100 2020/01/12

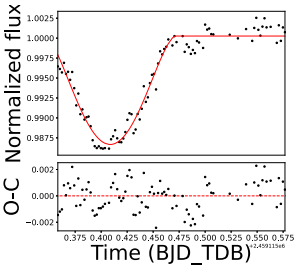

(b) T100 2020/09/22*

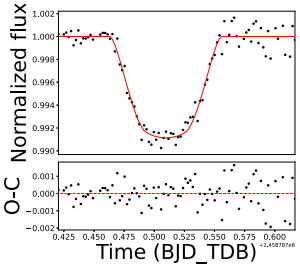

(c) T100 2019/10/30

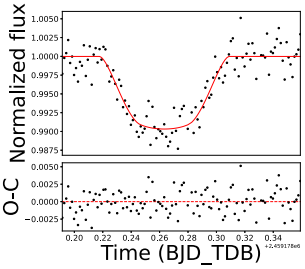

(d) T100 2020/11/24

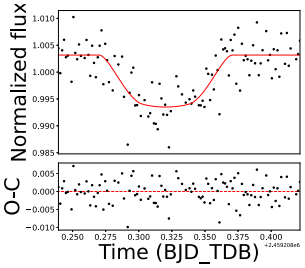

(e) UT50 2020/12/24

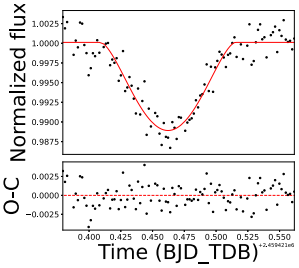

(f) T100 2021/07/25*

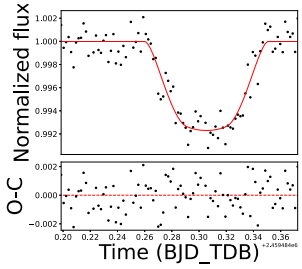

(g) ATA50 2021/09/26

Figure A14. WASP-93 b light curves.

APPENDIX B: LIST OF ETD OBSERVERS

We present the list of ETD observers in Table B1 with their unique TRESCA protocol number.

Table B1. ETD observers whose light curves were used in this study.

System	ETD number	Filter	Observer	TRESCA protocol number
GJ 1214	ETD44	Clear	Thomas Sauer	1278597072
GJ 1214	ETD48	*I*	Johannes Ohlert	1281369862
GJ 1214	ETD71	Clear	Esseiva Nicolas	1368129605
GJ 1214	ETD86	Clear	Fran Campos	1436715932
GJ 1214	ETD97	*I*	Marc Bretton	1531068175
GJ 1214	ETD105	Clear	Paul Benni	1616843398
HAT-P-1	ETD37	*R*	Ramon Naves	1378191469
HAT-P-1	ETD44	*V*	Marc Bretton	1506648757
HAT-P-10	ETD9	Clear	Luboš Brát	1252467945
HAT-P-10	ETD18	Clear	Samuel Durrance, Stacy Irwin	1292271351
HAT-P-10	ETD21	Clear	Luboš Brát	1317438434
HAT-P-10	ETD36	*R*	Mark Salisbury	1350197834
HAT-P-10	ETD39	Clear	Alfonso Carreno	1354463447
HAT-P-10	ETD44	Clear	Paul Benni	1380843090
HAT-P-10	ETD71	*R*	Ferran Grau Horta	1419237611
HAT-P-10	ETD85	Clear	David Molina	1476120518
HAT-P-10	ETD87	*R*	Wonseok Kang	1484834873
HAT-P-10	ETD88	*R*	Wonseok Kang	1484831725
HAT-P-10	ETD99	*V*	Yves Jongen	1544871912
HAT-P-10	ETD100	Clear	Bruno Fontaine	1546017209
HAT-P-10	ETD101	Clear	Yves Jongen	1567668774
HAT-P-10	ETD102	*R*	Veli-Pekka Hentunen	1569003995
HAT-P-10	ETD103	*V*	Yves Jongen	1569911364
HAT-P-10	ETD113	Clear	Matthieu Bachschmidt	1638791203
HAT-P-13	ETD39	*R*	Ramon Naves	1296839849
HAT-P-13	ETD82	Clear	Marc Bretton	1446972948
HAT-P-13	ETD100	Clear	Manfred Raetz	1579296693
HAT-P-13	ETD104	*R*	Manfred Raetz	1585809439
HAT-P-13	ETD107	*R*	Yves Jongen	1612792652
HAT-P-16	ETD10	*R*	Ruth ODougherty Sanchez	1291563452
HAT-P-16	ETD13	Clear	Stan Shadick	1318731754
HAT-P-16	ETD15	Clear	Jaroslav Trnka	1317463132
HAT-P-16	ETD16	*R*	Thomas Sauer	1317639008
HAT-P-16	ETD2	Clear	Jaroslav Trnka	1278846773
HAT-P-16	ETD23	*I*	Stan Shadick	1349233966
HAT-P-16	ETD27	*R*	Petri Kehusmaa, Caisey Harlingten	1351258657
HAT-P-16	ETD31	*R*	Mark Salisbury	1378590453
HAT-P-16	ETD36	Clear	Stan Shadick	1383606249
HAT-P-16	ETD37	Clear	Paul Benni	1383673356
HAT-P-16	ETD38	Clear	Anthony Ayiomamitis	1383875650
HAT-P-16	ETD39	*R*	Francesco Scaggiante, Danilo Zardin	1386236706
HAT-P-16	ETD45	Clear	Luca Rizzuti	1440519027
HAT-P-16	ETD46	Clear	David Molina	1446965044
HAT-P-16	ETD47	*R*	Fran Campos	1448107877
HAT-P-16	ETD5	Clear	Martin Vrašťák	1285498403
HAT-P-16	ETD57	*R*	Ramon Naves	1473584609
HAT-P-16	ETD59	Clear	Trnka J.	1477940875
HAT-P-16	ETD6	Clear	J. Világi, Š. Gajdoš	1288224520
HAT-P-16	ETD60	Clear	David Molina	1479143435
HAT-P-16	ETD61	*I*	Kevin B. Alton	1507651821
HAT-P-16	ETD63	*R*	Veli-Pekka Hentunen	1534770239
HAT-P-16	ETD64	Clear	Anael Wunsche	1537205125
HAT-P-16	ETD65	*R*	Josep Gaitan	1545555524
HAT-P-16	ETD69	*V*	Yves Jongen	1567852468
HAT-P-16	ETD70	*R*	Francesco Scaggiante, Danilo Zardin	1569339710
HAT-P-16	ETD70	*R*	Marco Fiaschi	1569339710
HAT-P-16	ETD7	*I*	Stan Shadick	1286159180
HAT-P-16	ETD72	*V*	Mario Morales	1571209785
HAT-P-16	ETD73	*V*	Truman State Observer	1583901308
HAT-P-16	ETD76	Clear	Anael Wunsche	1596031262
HAT-P-16	ETD78	*R*	Yves Jongen	1599988642
HAT-P-16	ETD79	*R*	Yves Jongen	1602144863
HAT-P-16	ETD80	*V*	Snaevarr Gudmundsson	1605914982
HAT-P-16	ETD9	Clear	Stan Shadick	1288134822

Table B1 – *continued*

System	ETD number	Filter	Observer	TRESCA protocol number
HAT-P-22	ETD53	*B*	Yves Jongen	1550908562
HAT-P-22	ETD55	*R*	Josep Gaitan	1552034513
HAT-P-22	ETD68	*R*	Manfred Raetz	1586181879
HAT-P-22	ETD78	*I*	Manfred Raetz	1614798234
HAT-P-22	ETD79	Clear	Matthieu Bachschmidt	1617521673
HAT-P-30	ETD14	Clear	Stan Shadick	1331321038
HAT-P-30	ETD15	*I*	Stan Shadick	1333050479
HAT-P-30	ETD16	Clear	Juanjo Gonzalez	1329671594
HAT-P-30	ETD18	*R*	Stan Shadick	1331919572
HAT-P-30	ETD22	Clear	Stan Shadick	1358100549
HAT-P-30	ETD26	*I*	Giuseppe Marino	1392576172
HAT-P-30	ETD30	*R*	Andre Christophe, Clement Jacques	1420878866
HAT-P-30	ETD30	*R*	Nougayrede Jean-Philippe	1420878866
HAT-P-30	ETD32	*R*	Marc Bretton	1425771388
HAT-P-30	ETD33	Clear	Martin Zibar	1425774283
HAT-P-30	ETD39	*R*	Francesco Scaggiante, Danilo Zardin	1516875191
HAT-P-30	ETD41	Clear	Marc Bretton	1519263504
HAT-P-30	ETD47	*V*	Yves Jongen	1580746869
HAT-P-30	ETD51	Clear	Marc Bretton	1586081207
HAT-P-30	ETD52	*R*	Yves Jongen	1607422166
HAT-P-30	ETD53	*R*	Jean-Claude Mario	1607859317
HAT-P-30	ETD55	*R*	Yves Jongen	1612549479
HAT-P-30	ETD56	*R*	Yves Jongen	1612791934
HAT-P-30	ETD58	*R*	Josep Gaitan	1613042887
HAT-P-30	ETD59	*R*	Anael Wunsche	1613037601
HAT-P-53	ETD11	*R*	P. Farissier, S. Combe, L. Bret-Morel	1463150362
HAT-P-53	ETD11	*R*	C. Gillier, R. Montaigut	1463150362
HAT-P-53	ETD18	Clear	Marc Bretton	1480634960
HAT-P-53	ETD4	Clear	Marc Bretton	1440128332
HAT-P-53	ETD43	Clear	Marc Deldem	1600626997
HAT-P-53	ETD45	Clear	Yves Jongen	1599293169
HAT-P-53	ETD48	Clear	Manfred Raetz	1605559616
HAT-P-53	ETD50	*R*	Jordi Lopesino	1609010356
KELT-3	ETD2	*R*	Ramon Naves	1357282983
KELT-3	ETD20	*V*	Marc Bretton	1428978215
KELT-3	ETD24	Clear	David Molina, Antoni Vives Sureda	1461153031
KELT-3	ETD29	*R*	Josep Gaitan	1553504934
KELT-3	ETD3	Clear	Anthony Ayiomamitis	1362940487
KELT-3	ETD6	Clear	Paul Benni	1387025732
KELT-3	ETD9	Clear	Gustavo Javier, Muler Schteinman	1393492000
QATAR-2	ETD19	Clear	Nico Montigiani, Massimiliano Mannucci	1335686620
QATAR-2	ETD30	Clear	C. Colazo, R. Melia, N. Marcionni	1369893611
QATAR-2	ETD37	Clear	Thomas Sauer	1403609906
QATAR-2	ETD70	Clear	Yves Jongen	1581427637
QATAR-2	ETD83	Clear	Yves Jongen	1591620453
QATAR-2	ETD87	Clear	Yves Jongen	1618771546
QATAR-2	ETD90	Clear	Yves Jongen	1619795469
WASP-8	ETD2	*R*	Yves Jongen	1605261835
WASP-44	ETD12	Clear	Bernasconi Laurent	1477991767
WASP-44	ETD18	IR-UV	Yves Jongen	1538296133
WASP-44	ETD2	Clear	Phil Evans	1315683470
WASP-44	ETD20	Clear	Laloum Didier	1569947071
WASP-44	ETD22	IR-UV	Yves Jongen	1594936390
WASP-44	ETD23	*R*	Yves Jongen	1596286136
WASP-44	ETD25	Clear	Yves Jongen	1626442442
WASP-44	ETD26	*V*	Anael Wunsche	1626433743
WASP-44	ETD27	Clear	Yves Jongen	1627914023
WASP-44	ETD4	Clear	František Lomoz	1316937777
WASP-44	ETD5	*R*	Thomas Sauer	1342738906
WASP-44	ETD6	Clear	Phil Evans	1380404329
WASP-44	ETD7	Clear	Rene Roy	1386089485
WASP-50	ETD11	*V*	Christopher Allen	1354306402
WASP-50	ETD16	*V*	Vanessa Logan, Karen Lewis	1392655969
WASP-50	ETD18	Clear	Esseiva Nicolas	1384452957

Table B1 – *continued*

System	ETD number	Filter	Observer	TRESCA protocol number
WASP-50	ETD29	*V*	Andrew Stewart	1494365750
WASP-50	ETD3	Clear	Fernando Tifner	1320032307
WASP-50	ETD33	*R*	Tianyu Ma	1479154021
WASP-50	ETD36	Clear	Bernasconi Laurent	1478164712
WASP-50	ETD37	*R*	Christoper Michael	1481483736
WASP-50	ETD4	Clear	Parijat Singh	1323109321
WASP-50	ETD44	Clear	C. Colazo, R. Melia, M. Starck	1514898205
WASP-50	ETD45	*R*	Marc Bretton	1542158605
WASP-50	ETD55	*V*	Yves Jongen	1575812213
WASP-50	ETD56	*V*	Yves Jongen	1579635308
WASP-50	ETD57	*R*	Yves Jongen	1601116953
WASP-50	ETD58	*R*	Yves Jongen	1601412777
WASP-50	ETD59	*R*	Yves Jongen	1601502007
WASP-50	ETD6	*V*	Nicole Makely, Melissa Hutcheson	1340302725
WASP-50	ETD60	*R*	Yves Jongen	1605913925
WASP-50	ETD63	Clear	Esseiva nicolas	1606397868
WASP-77	ETD1	Clear	Juanjo Gonzalez	1376989484
WASP-77	ETD16	Clear	David Molina	1475258342
WASP-77	ETD18	*I*	Phil Evans	1478155148
WASP-77	ETD2	Clear	Paul Benni	1383268828
WASP-77	ETD22	*R*	Josep Gaitan	1481360368
WASP-77	ETD23	Clear	Š. Gajdoš, J. Šubjak	1488671491
WASP-77	ETD24	*V*	Napoleao T., Silva S., Kulh D.	1539901020
WASP-77	ETD27	*R*	Pavel Pintr	1578518743
WASP-77	ETD28	*R*	Yves Jongen	1596751821
WASP-77	ETD29	*R*	Yves Jongen	1602265968
WASP-77	ETD3	Clear	Paul Benni	1385854480
WASP-77	ETD30	*R*	Yves Jongen	1602850422
WASP-77	ETD6	*V*	Ferran Grau Horta	1386541771
WASP-93	ETD21	*R*	Mark Salisbury	1509911995
WASP-93	ETD42	*V*	Yves Jongen	1569913117
WASP-93	ETD49	*R*	Josep Gaitan	1601800673
WASP-93	ETD8	*R*	Mark Salisbury	1475784797
WASP-93	ETD9	Clear	Marc Deldem	1475523697
XO-2	ETD71	*R*	Ramon Naves	1295965000
XO-2	ETD77	*R*	Thomas Sauer	1300726462
XO-2	ETD110	*R*	Jacques Michelet	1364137719
XO-2	ETD124	Clear	Martin Zibar	1429649013
XO-2	ETD132	Clear	Trnka J.	1483125364
XO-2	ETD133	*R*	Wonseok Kang	1484831673
XO-2	ETD142	Clear	Stan Shadick	1522015555
XO-2	ETD143	*I*	Marc Bretton	1523058603
XO-2	ETD154	Clear	Joe Garlitz	1552959381
XO-2	ETD170	Clear	Manfred Raetz	1585437743
XO-2	ETD172	*R*	Manfred Raetz	1586597501

APPENDIX C: LIST OF INFORMATION ABOUT LIGHT CURVES ANALYSED IN THIS STUDY

We present the detailed information about the light curves analysed in this study in Table C1 for GJ 1214 system. Same table for other systems within this study can be found in online material of the journal with a read-me file describing the columns.

Table C1. Detailed information about GJ 1214 light curves analyzed in this study.

Beta	PNR (ppt)	Source	Depth	T_{14}	T_c error	$T_{ingress/egress}$ error	Depth error	$T_{ingress/egress}$	T_c (BJD_TDB)	Filter	Type	Discard	Removed	Epoch	O-C (min.)	Linear Residual (min.)
1.54002179740703	2.90501157258658	ETD44	0.01918	0.039077	0.00038267613	0.001325629	0.00059327354	0.010842	2455385.3323	Clear	ETD	10	1			
1.41497140877592	1.56266457657402	ETD48	0.015165	0.038365	0.00017306575	0.00059951733	0.00025728618	0.006539	2455396.395716	I	ETD	0	0	−255	−1.75953648984432	0.504614573294904
1.95335549554965	1.12704441253944	ETD71	0.014853	0.044947	0.00066474353	0.0023027391	0.00075196981	0.009814	2456420.497064	Clear	ETD	0	0	393	−3.16405445337296	−0.503744903729233
1.73996684084739	1.02451060166468	ETD86	0.014383	0.035416	0.00079393994	0.0027502886	0.0014203748	0.004132	2457215.438891	Clear	ETD	1	1	896	−5.752396881580 35	−2.78457468612666
1.44406723953075	3.01927543583687	ETD97	0.016271	0.038981	0.00032347593	0.0011205535	0.00054037784	0.005701	2458307.500585	I	ETD	0	0	1587	−2.92512930929661	0.465140108076548
1.92712266700976	2.17085192544031	ETD105	0.015684	0.037229	0.00039431705	0.0013659543	0.00063640066	0.00606	2459296.833314	Clear	ETD	0	0	2213	−3.916310146451	−0.14333166840985
2.19062931990964	1.23194238093312	Kundurthy et al. 2011	0.014553	0.036928	0.000090594633	0.00031382901	0.0001491875	0.004873	2455307.892618	sdssr	Literature	0	0	−311	−2.37597115337849	−0.146056044548218
0.971768878384822	4.69936153795429	Cáceres et al. 2014	0.014276	0.03705	0.00007518823	0.00026045967	0.00012155812	0.004842	2455315.794883	I	Literature	0	0	−306	−2.029075026512 15	0.20389686395285
2.22060231209693	2.40455477107574	Harpsøe et al. 2013	0.015432	0.038471	0.00040131617	0.0013902	0.00064413727	0.005629	2455315.794995	sdssi	Literature	0	0	−306	−1.86779513955116	0.365176750913834
2.01714726205399	1.27922416375966	de Mooij et al. 2012	0.014329	0.036998	0.00029215788	0.0010120646	0.00044607319	0.005613	2455342.661299	r	Literature	0	0	−289	−2.70002894103527	−0.456663993012198
0.696405871852179	7.38398165051281	de Mooij et al. 2012	0.014834	0.039589	0.00023377536	0.00080982162	0.00031854505	0.007352	2455342.661793	K	Literature	0	0	−289	−1.98866888888073	0.254696059215776
1.3826047750966	1.43953200388388	Kundurthy et al. 2011	0.015961	0.037895	0.00013967494	0.00048384818	0.00022323204	0.006317	2455353.72466	sdssr	Literature	0	0	−282	−1.94077469408512	0.306869748226572
1.878081483 1968	1.36481470615678	de Mooij et al. 2012	0.013867	0.03667	0.00011052198	0.00038285939	0.00018239978	0.004372	2455380.590935	sdssz	Literature	0	0	−265	−2.81476847827435	−0.556730978404576
2.10949846638068	3.46390953487826	de Mooij et al. 2012	0.015661	0.038892	0.00027134763	0.00093997577	0.00043878893	0.005642	2455380.591226	sdssg	Literature	0	0	−265	−2.39572830498219	−0.137690805112416
2.05667039841214	1.47624912995891	de Mooij et al. 2012	0.014576	0.037102	0.00011544754	0.00039992201	0.00018461769	0.00521	2455380.591233	sdssi	Literature	0	0	−265	−2.38564789295197	−0.127610393082196
2.08973252119274	1.73520024460113	de Mooij et al. 2012	0.015226	0.03786	0.00013581942	0.00047049229	0.00021688722	0.005644	2455380.591281	sdssr	Literature	0	0	−265	−2.31652803719044	−0.058490537320668
2.05904592219586	0.534642565539024	Harpsøe et al. 2013	0.015424	0.0368	0.00021331088	0.00073893055	0.00035358795	0.005539	2455383.751738	I	Literature	0	0	−263	−2.82432921230793	−0.565068999784269
1.51246622946044	1.1554119947922	Kundurthy et al. 2011	0.01502	0.037032	0.000086850798	0.00030085999	0.00014450977	0.005104	2455383.752222	sdssr	Literature	0	0	−263	−2.12736926972866	0.131890942795
3.841729 41469478	0.751229700687564	Harpsøe et al. 2013	0.015354	0.037664	0.0001518402	0.00052598987	0.00024378328	0.005727	2455391.654123	I	Literature	1000	1			
1.97141158071663	0.399557185466158	de Mooij et al. 2012	0.014209	0.036406	0.000052885215	0.00018319976	0.000088523117	0.00452	2455407.458131	I	Literature	0	0	−248	−2.36252188682556	−0.094091329397716
2.27061228061283	0.727728845059969	Harpsøe et al. 2013	0.013467	0.036102	0.00010720389	0.00037136516	0.0001832348	0.00385	2455410.618996	I	Literature	0	0	−246	−2.28280328214169	−0.013150012059949
0.973337378964746	1.22441688249975	Harpsøe et al. 2013	0.014379	0.036766	0.00020088622	0.00069589029	0.00034969884	0.004189	2455415.360198	sdssi	Literature	0	0	−243	−2.30074591934681	−0.029258580284235
0.878990098512957	9.07091893117274	de Mooij et al. 2012	0.015473	0.040469	0.00024503472	0.00084882517	0.00029323522	0.011569	2455426.424175	K	Literature	1	1	−236	−0.654451623558998	1.6213152097922
2.359963256300 05	0.955226712305003	Harpsøe et al. 2013	0.014877	0.038469	0.00015059533	0.00052167754	0.00023111066	0.005743	2455429.583803	I	Literature	0	0	−234	−2.35601283609867	−0.079023290093586
0.822571989863981	2.11830531885857	Gillon et al. 2014	0.013214	0.038119	0.00015918695	0.00055143977	0.00023098113	0.005009	2455631.875896	I+z	Literature	0	0	−106	−1.95851549506187	0.396727660792257
1.19576695807761	2.34075571461259	Gillon et al. 2014	0.015162	0.039121	0.00001401945	0.000485648	0.00021465065	0.005905	2455650.840331	I+z	Literature	0	0	−94	−2.56740443408489	−0.204825002307413
0.8899489 10909974	2.33257626757927	Gillon et al. 2014	0.013247	0.036393	0.00013005906	0.0004505378	0.00021279607	0.004054	2455669.805516	I+z	Literature	0	0	−82	−2.09629453718662	0.273621170514205
0.924076675512996	3.63757122017 35	Gillon et al. 2014	0.013795	0.037471	0.00020290215	0.00070287368	0.00031045503	0.005008	2455677.707187	I+z	Literature	0	0	−77	−2.60475888848305	−0.231786399147492
1.22130279062034	2.80072205362528	Gillon et al. 2014	0.014631	0.037079	0.00013958613	0.00048354052	0.00023842143	0.004505	2455680.868054	I+z	Literature	0	0	−75	−2.52215959131718	−0.14796438932773
0.692314390641076	2.60511774796333	Gillon et al. 2014	0.013419	0.037949	0.00018892815	0.00065446631	0.00027064594	0.00539	2455696.672245	I+z	Literature	0	0	−65	−2.31652803719044	0.063780728068466
1.01307130172199	2.85798065969031	Gillon et al. 2014	0.013381	0.035668	0.00014302326	0.00049544709	0.00024871441	0.003705	2455699.832824	I+z	Literature	0	0	−63	−2.64864921569824	−0.267117737785447
2.36197219818054	1.01691316576869	Harpsøe et al. 2013	0.015037	0.037554	0.00016333706	0.00056581619	0.00025973646	0.005596	2455715.637167	R	Literature	0	0	−53	−2.22413800656795	0.163507034614297
0.911384333866416	13.8641033490619	Cáceres et al. 2014	0.013403	0.038567	0.00030249204	0.0010478632	0.00043304365	0.005264	2455783.594092	2.14um_narrow	Literature	100	1			
1.12302264232073	1.3331571169042	Narita et al. 2013	0.014135	0.036622	0.00011724402	0.00040614518	0.00019946084	0.004268	2455788.335846	J	Literature	0	0	−7	−2.14165471494198	0.274112717279774
1.14779098301767	1.33915400192187	Narita et al. 2013	0.014311	0.03661	0.00011778865	0.00040803185	0.00019996286	0.004414	2455788.335853	H	Literature	0	0	−7	−2.13157497346401	0.284192458757741
1.57806255042784	1.63289139587076	Narita et al. 2013	0.013572	0.036857	0.00016212056	0.0005616021	0.00024613037	0.005021	2455788.336052	K	Literature	0	0	−7	−1.84501446783543	0.570752964386327
1.82989108161083	2.399880960675	Harpsøe et al. 2013	0.015027	0.03773	0.00038349532	0.00132846 68	0.00057729311	0.006351	2455799.398034	sdssz	Literature	0	0	0	−3.07152025401592	−0.65147332750555
1.8052699833899	2.014839973388 65	Harpsøe et al. 2013	0.014445	0.037417	0.0003181385	0.0011020641	0.00049451349	0.005393	2455799.398567	sdssg	Literature	0	0	0	−2.30400010943413	0.116046817076245
1.91651897753165	1.45359009666968	Harpsøe et al. 2013	0.013746	0.036933	0.00019493565	0.00067527691	0.00033452789	0.003883	2455799.398769	sdssr	Literature	0	0	0	−2.01311990618706	0.406927020323315
2.00010592202447	0.561661977317683	Nascimbeni et al. 2015	0.013604	0.036075	0.00004483982	0.00015532969	0.000077179109	0.00388	2456015.913815	R	Literature	0	0	137	−2.60976925492287	−0.105966511620937
1.7167103167892	1.38303539212177	Nascimbeni et al. 2015	0.014552	0.036797	0.00014755908	0.00051115965	0.00022948456	0.005616	2456015.914246	B	Literature	0	0	137	−1.98912955820 56	0.514673185096325
1.66744508440514	0.742537137178145	Nascimbeni et al. 2015	0.018167	0.039255	0.00014449 47	0.00050054431	0.0002190867	0.009722	2456064.906315	B	Literature	0	0	168	−2.68093429505825	−0.158179505621005
1.62895253396986	0.581737296919655	Nascimbeni et al. 2015	0.013822	0.036978	0.000050122408	0.00017362911	0.000079720591	0.004676	2456064.906354	R	Literature	0	0	168	−2.62477487325668	−0.102020083819438
1.00859192594658	2.13477762122242	20220512 T80	0.012126	0.036145	0.00022431826	0.00077706125	0.00035440397	0.003622	2455701.413994	iprime	our	0	0	−62	−1.54679037630558	0.835352457934161
1.11617964439914	3.51947548154011	20200611 T100	0.015828	0.039198	0.00037575773	0.0013	0.00061163715	0.005634	2459012.360728	R	our	0	0	2033	−3.51080641150475	0.15212792768618
2.08267303466749	3.00169245738781	20200703 T100	0.015081	0.037681	0.00045417007	0.00157329 13	0.00072708222	0.005518	2459034.486291	I	our	0	0	2047	−3.66125755012035	0.010235777647812
1.97247862626836	2.33689387413991	20210423 T100	0.014749	0.037149	0.00026050322	0.00090240961	0.00041434169	0.00542	2459328.441673	I	our	0	0	2233	−3.53816628456116	0.247039320018903
2.00285455916959	2.60556008694825	20210719 T100	0.021252	0.050181	0.00045961826	0.0015921643	0.00053107098	0.02509	2459415.362554	I	our	10	1			

This paper has been typeset from a TEX/LATEX file prepared by the author.